Kent Academic Repository
Full text document (pdf)

Citation for published version

Foglia, Fabrizia and Karan, Santanu and Nania, Manuela and Jiang, Zhiwei and Porter, Alexandra E. and Barker, Robert and Livingston, Andrew G. and Cabral, João T. (2017) Neutron Reflectivity and Performance of Polyamide Nanofilms for Water Desalination. Advanced Functional Materials, 27 (37). ISSN 1616-301X.

DOI

https://doi.org/10.1002/adfm.201701738

Link to record in KAR

https://kar.kent.ac.uk/65791/

Document Version

Author's Accepted Manuscript

Neutron reflectivity and performance of polyamide nanofilms for water desalination

Fabrizia Foglia, Santanu Karan, Manuela Nania, Zhiwei Jiang, Alexandra E. Porter, Robert Barker, Andrew G. Livingston, João T. Cabral*

Fabrizia Foglia, Santanu Karan, Manuela Nania, Zhiwei Jiang, Andrew G. Livingston, João T. Cabral
Department of Chemical Engineering, Imperial College London, London SW7 2AZ, UK.
E-mail: j.cabral@imperial.ac.uk
Fabrizia Foglia
Current address: Institute of Pharmaceutical Science, King's College London, London, UK.
Alexandra E. Porter,
Department of Material, Imperial College London, London SW7 2AZ, UK.
Robert Barker
Institut Laue Langevin, 38042, Grenoble, France.
Current address: School of Science and Engineering, University of Dundee, Dundee, UK.

We investigate the structure and hydration of polyamide membranes, with a combination of neutron and X-ray reflectivity, and benchmark their performance in reverse osmosis water desalination. PA membranes were synthesised by the interfacial polymerization of m-phenylenediamine (MPD) and trimesoyl chloride (TMC), varying systematically reaction time, concentration and stoichiometry, to yield large-area exceptionally planar films of ≈10 nm thickness. Reflectivity was employed to precisely determine membrane thickness and roughness, as well as the (TMC/MPD) concentration profile, and response to hydration in the vapour phase. PA film thickness was found to increase linearly with reaction time, albeit with a non-zero intercept, and the composition cross-sectional profile was found to be uniform, for the conditions investigated. Furthermore, H_2O and D_2O vapour hydration from 0 to 100% relative humidity resulted in considerable swelling (up to 20%), but also yielded uniform

cross-sectional profiles. The resulting film thickness is found to be predominantly set by the MPD concentration, while TMC regulates water uptake. A favourable correlation is found between higher swelling and water uptake with permeance. Our data provide quantitative insight into the film formation mechanisms and correlate reaction conditions, cross-sectional nanostructure and performance of the PA active layer in RO membranes for desalination.

1. Introduction

Separation processes represent approximately 45% of energy usage in downstream petrochemical and manufacturing processes,[1] with membrane-based separations generally offering efficient strategies to decrease energy requirements and environmental footprint.[1]

Specifically, as less than 1% of the Earth's water is considered to be 'fresh',[2] desalination and waste water treatments are pressing societal challenges, required to meet the growing demand for fresh water for human consumption, agriculture and industry. These are increasingly met by membrane processes, including reverse osmosis (RO), nanofiltration (NF), and electrodialysis (ED), over traditional thermal and vacuum distillation technologies. Over the past decades, membrane performance for water desalination has improved by a few orders of magnitude, while maintaining economically attractive productivities.[3] In recent years, RO has emerged as the leading membrane technology for new desalination plants for both brackish and sea water, as well as in wastewater treatment and organic contaminant removal.[2-9]

A major challenge faced by RO membrane technologies remains, however, a reduction in energy consumption, associated with the required operation pressure, and a reduction in performance losses during operation, in order to improve process efficiency.[10-12] Further, variations in water supply (including salinity and foulants), plant location, pre-treatment and waste disposal requirements, demand RO membrane and process optimization tailored for the

specific context.[13-15] Despite considerable research in RO membrane structure and transport,[10] our fundamental understanding and thus ability to achieve high selectivity (in addition to high permeability) and thus reduce the energy consumption of separation processes and improve performance[16-17] remains limited and progress has been largely empirical.[10]

Reverse Osmosis (RO) membranes comprise a 'tight' separating polymeric layer on a more 'open' support layer (generally polysulfone), mounted on a woven fabric backing (generally polyester).[10,18-20] The separating or active layer is usually manufactured by interfacial polymerization (IP) at the organic/aqueous interface between an aromatic diamine (*m*-phenylenediamine, MPD) and trimesoyl chloride (TMC). IP is a polycondensation process between two multifunctional monomers dissolved in immiscible solvents (generally an aqueous and an organic phase) that takes place at the interface between the two solvents. Formally, the organic-soluble component (acid chloride) is insoluble into the polymer, whereas the water-soluble component (diamine) diffuses through the film to react with the acid chloride at the film/organic phase interface, where the film grows.[21-22] The resulting cross-linked polyamide (PA) film has an overall "apparent" film thickness of, typically, a few hundred nm, and is rough and crumpled, with individual PA film thickness of the order of 10 nm, as revealed by recent high resolution imaging reports,[23-26] supported by a porous polysulfone layer with a heterogeneous nanoscale interface layer.[27]

Despite being widely used on an industrial scale, membranes obtained via IP are generally inhomogeneous in terms of spatial variation, chemistry and porosity at the micrometer to nanoscales.[28-29] Although the interplay between the top layer and porous support is important for the membrane properties and, for instance, the support layer undergoes compaction during operation[10] thus contributing to a reduction in flux, the actual separation process is governed by the skin PA layer. Therefore, a molecular-level understanding of the structure and chemistry[25,28-31] of this layer

appears to be critical to enable the design of novel membranes with superior water desalination performance.[25,30-31] Towards this goal, considerable effort has been dedicated to the structural characterization of the skin layer of commercially available RO membranes,[26,28-37] generally carried out under vacuum (away from operating conditions), molecular modelling,[38-43] or by developing more controlled synthetic pathways.[37,44-48] These include: spin-assisted molecular layer-by-layer (mLbL) techniques,[37,44-45] and ultrathin films synthesized on $Cd(OH)_2$ nanowires[46] and carbon nanotube supports,[47] or a cellulose nanocrystal interlayer,[48] seeking to fabricate highly controlled PA thin films, and systematically correlate film thickness, roughness and membrane performance. By tuning the reaction stoichiometry and time, and thus roughness, a favourable correlation between surface area and membrane flux has been proposed,[46] suggesting a powerful route to manufacture thin film membranes with high permeance. Crumpled nanofilms polymerized under such controlled interfacial reaction conditions yielded acetonitrile permeances up to 112 L m^{-2} h^{-1} bar^{-1}, two orders of magnitude higher than those of commercially available membranes at equivalent solute retention.[46]

Since commercial RO membranes typically exhibit a complex, undulated crumpled structure comprising thin films of local thickness of the order of 10 nm, this synthetic route opens possibilities for the direct examination of individual nanofilms within the active layer. With this in mind, our paper seeks to elucidate the nanoscale structure of single PA films, and specifically resolve (i) the cross-sectional composition profile resulting from IP of TMC and MPD and (ii) the membranes response to water, in terms of dimensional changes and the distribution of water throughout the sample, and (iii) evaluate possible correlation with performance.

The planarity and uniformity of the membrane films of ~10 nm thickness, with footprint in excess of several cm^2, enables us, for the first time, to employ neutron and

X-ray reflectivity to probe the active layer of PA membranes, directly relevant to the RO separation processes. X-ray reflectivity allows a robust quantification of the film thickness and roughness, as well as the scattering length density (SLD) profile with Å resolution.[35-37,44-45] Combined with neutron reflectivity and isotopic contrast variation, we are able to resolve the membrane structure and selectively elucidate its various components, under dry and hydrated states, for various reactant stoichiometries and reaction times. Assisted with molecular dynamics simulations and membrane salt rejection and flux measurements, a comprehensive molecular model of PA active layer structure and its relation to performance emerges.

2. Results and Discussion

2.1. Dry PA

The fabrication of PA nanofilms by nanowire-supported IP is illustrated in **Figure 1**a (detailed in Figure S1), yielding thickness of the order of 10 nm (**Figure 1**b), commensurate with film thicknesses of corrugated PA skin layers in RO membranes (**Figure 1**c). These planar thin films, with sub-nm surface roughness (detailed in Figure S2), were subsequently floated and transferred onto polished silicon wafers for characterization via reflectometry.

X-ray and neutron reflectivity were employed to elucidate the mechanism of membrane formation, the evolution of film thickness, its possible asymmetry and heterogeneity associated with IP, and response to the ingress of water, with Å resolution. It has been suggested that IP proceeds via cluster formation, aggregation and percolation[40,43,49-50] which have been analytically and numerically modelled. *Karode et al.*[51] proposed that TMC/MPD "polymer primarily particles" (oligomeric clusters) are initially formed and then coalesce to yield a "coherent film", *via* a nucleation process which is concentration dependent.

The initial stage is thought to evolve as a diffusion-limited aggregation (DLA) process, creating dense "colloidal" particles, with active functional groups at the surface, which then aggregate into a lower density structure.[49-50] The latter yields an inhomogeneous film, exhibiting functional group asymmetry and surface polarization.[40]

Upon film formation, reactant transport from the aqueous phase across the incipient film barrier becomes severely hindered, limiting further film growth at the organic interface. As a result, the evolution of film thickness with time is highly non-linear, comprising an initial fast regime, followed by a much slower, asymptotic growth stage. Predictions for the limiting film thickness and the asymmetric distribution of density and charge have been proposed.[49]

Experimentally, we precisely resolve the dependence of film thickness with reaction time, between 1 to 20 min, and TMC/MPD stoichiometry, as shown in **Figure 1**. We have selected reagent concentrations and stoichiometries that lead to flat PA membranes, yet with films with thicknesses comparable to single skin folds of ubiquitous crumpled PA membranes, extensively employed industrially, and with reasonable performance. From a reference reagent ratio TMC/MPD 0.005/0.1 wt% (shown in blue), we explore permutations by changing one reactant concentration at a time, specifically to 0.005/1 (green) and 0.05/0.1 wt% (red).The NR profile for TMC/MPD (shown here for 0.005/0.1 wt%), depicted in **Figure 1**d is well described by a single layer with approximately uniform density across the film cross-section, shown in **Figure 1**e, whose thickness increases linearly within the window of reaction times investigated (detailed in Table S1). A linear extrapolation to reaction time zero would yield fim thickness between 6-8 nm for the various stoichiometries. For TMC/MPD 0.005/0.1 wt%, shown in **Figure 1**f, we obtain that the the film thickness grows as $h = 0.24 t + 6.93$, where h is in [nm], and t is reaction time in [min], within the time window probed. However, at reaction times shorter than 1 min, we do not reliably obtain coherent films with mechanical integrity. These observations corroborate the highly non-linear nature of the film

growth mechanism,[31] and quantify the IP kinetics. We interpret the initial stage to correspond to the cluster formation, reaching a coherent film at approximately 1 min reaction time, when measurements are first possible, at these low reactant concentrations. We resolve a considerable time window of linear growth, indicating that asymptotic self-limiting growth, expected due to restriction of amine diffusion accross the film,[31] occurs at even longer reaction times.

Further, the membrane film densifies within these reaction times, as shown by the increase of the characteristic film SLD, shown in **Figure 1**e, from which the mass density can also be evaluated (Figure S3). The SLD values obtained are compatible with a fully cross-linked structure with a ratio TMC/MPD 2:3 (Figure S1i), previously measured by XPS on identical membranes.[46] Upon increasing MPD reactant concentration, the resulting film thickness (at fixed reaction time) increases considerably, as shown in **Figure 1**g, while the variation in TMC concentration by one order of magnitude has a negligible effect on h, as shown in **Figure 1**h (detailed in Figures S4 and S5 and in Table S1).

Hydrogenous TMC/MPD membranes do not enable an evaluation of compositional asymmetry of the membrane along the cross-section, due to limited neutron contrast. This can be resolved by selective deuteration of one component, MPD in our case, and NR data and SLD profile are shown in **Figure 1**i-j. The observed profile indicates a homogenous distribution of MPD and TMC across the film cross-section. The simultaneous analysis of the hydrogenous and partially deuterated contrasts enables an unambiguous resolution of the IP film cross-section, showing no selective enrichment of components at either interface. More complex (e.g. multi-layer) models did not result in a meaningful improvement of the agreement with the data, in either the fully hydrogenous or the partially deuterated case, and were therefore not explored further. All investigated reaction times and stoichiometries yield planar films with sub-nm surface roughness and homogeneous composition along the film cross-section. We note, however, that NR measurements are averaged over the relatively large

beam footprint (2x2 cm^2) and thus local (compositional or density) variations within the plane of the film are not resolved. Further, composition variations at the film's top and bottom interfaces, if any, can be estimated to be smaller than the interfacial roughness of <1 nm in all cases (detailed in Figures S2 and S3 and in Table S1).

Collectively, these data provide unique insight into the cross-sectional structure of the PA active layer with Å resolution. The non-linear evolution of film thickness and composition homogeneity across the film thickness (~10 nm) is compatible with the IP models of clusters formation and self-limiting growth, enabling quantitative comparison with simulation[40-41] and modelling.[49,51]

2.1. Hydrated PA

We next consider the hydration of PA membranes, focusing on the thin film swelling and water uptake, as well as the possible change in density and water distribution along the film cross-section. We systematically probe the film structure at increasing hydration in an enclosed humidity chamber from 0 to 100% RH. In order to increase measurement precision, we hydrate with heavy water (D_2O). We compute the water uptake independently from the variation in SLD and thickness of the hydrated film h_{RH} as follows. The SLD of the dry PA film is $SLD_{PA} = (n_{PA} N_A \Sigma b_{PA})/(h_{RH=0} A)$, where n_{PA} is the number of moles of one PA unit ($C_{18}H_{12}O_3N_3$) in the measured sample volume, with corresponding neutron scattering length b_{PA}; the scattering volume is formally expressed as $h_{RH=0} A$, the product of film thickness at fixed beam footprint A; N_A is Avogadro's number. Upon hydration, the SLD of the film becomes:

$$SLD_{RH} = (n_{PA} N_A b_{PA})/(h_{RH} A) + (n_{D2O} N_A b_{D2O})/(h_{RH} A) \tag{1}$$

where b_{D2O} and n_{D2O} are the scattering length and number of moles of D_2O in the measured volume, respectively. The hydrated volume is now $h_{RH} A$. Evidently n_{PA} remains constant while n_{D2O} increases upon hydration, and we define water uptake as the molar ratio n_{D2O}/n_{PA}.

From the measured film thickness and initial sample mass, the overall and partial densities can be computed as:

$$\rho_{TOT(RH)} = \rho_{PA(RH)} + \rho_{D2O(RH)} = (n_{PA}M_{w(PA)})/(h_{RH}A) + (n_{D2O}M_{w(D2O)})/(h_{RH}A) \qquad (2)$$

where $M_{w(PA)}$ and $M_{W(D2O)}$ are the molar masses of the PA unit and D_2O. The value of A is implicit in these calculation, since n are estimated directly from SLD.

NR data for three stoichiometries, at selected reaction time 10 min, are shown in **Figure 2**a-c. The corresponding SLD profiles, **Figure 2**d-f, quantify the membrane swelling and increase in film SLD with RH, from which the water uptake can be determined (detailed in Figure S6, Tables S1 and S2). The constant SLD value along the film cross-section, at all RH and stoichiometries, unambiguously indicates that water is homogenously distributed along the direction normal to the film surface (on average, across the plane of the membrane). This finding is in agreement with the observed TMC/MPD composition homogeneity discussed above.

Upon cycling RH, no hysteresis in the data is observed, indicating a reversible and quasi-equilibrium structural response upon membrane hydration and dehydration (at the timescale of several min). These results are corroborated by complementary XRR studies (Figure S7), which further improve the quantification of both h and roughness, owing to the large SLD contrast.

The dry SLD values for films prepared at all reagent stoichiometries are approximately identical, which indicate that the TMC/MPD 2:3 film ratio applies to all conditions. However, the SLD values in each case evolve differently upon hydration which, qualitatively, indicates that the PA film density and/or water uptake with RH depends on reagent stoichiometry. Careful modelling of the NR data enables the quantification of the changes in hydrated film thickness h_{RH} as well as overall and partial densities, and thus decoupling water uptake from film swelling.

These measurements seek to shed light on the packing and free-volume[52] of PA RO membranes and thus finding correlations with solute transport.

Irregular packing and local structural and compositional heterogeneity is predicted to occur during the membrane-formation, and thus create density modulations and porosity.[52] Such voids can be expected to be varying in circularity, openess and connectivity, and change with treatments such as conditioning, annealing, swelling and/or pressurization.[52] Indeed, a discrepancy between the degree of membrane swelling and volume fraction of water uptake has been reported.[50-52]

Previous molecular dynamics (MD) and Monte Carlo (MC) simulations,[41,50] and positron annihilation lifetime spectroscopy (PALS) studies[53] suggest that fully cross-linked PA film exhibit a distribution of cavity sizes, with dimensions of the order of 5 Å, which remains broadly unchanged along the direction normal (z) to the membrane surface, becoming slightly larger at both interfaces. *Kim et al.*[53] detected a bimodal pore distribution, of "network" and "aggregate" pores, the former being smaller and related to the geometry of the crosslinked network and the latter being larger and related to film formation. For instance, the addition of DMSO in the aqueous phase during IP has been found to increase the size and number of network pores and thus increase flux.[53] Along the plane (xy) of the membrane, water is thus expected to be distributed heterogeneously within the polymeric matrix.[54]

Our reflectivity results, from which the polymer density and water distribution can be computed, reveal that both are homogeneous along the film normal direction (z), with Å resolution. Lateral (xy) heterogeneity at the nanoscale is not directly probed, as the measurements are averaged over a large representative (illuminated) area with a footprint exceeding cm^2. Our SLD profiles of both dry and hydrated PA films indicate uniform polymer and water distributions at all conditions, on average, along the z-direction, and no evidence of possibly larger or more numerous pores (and possibly water) at either interface. While the measurements presented so far were carried out under controlled hydration conditions,

supplementary experiments were performed under direct immersion in water yielding similar results with 100% RH (Figure S8).

Quantitative analysis of the SLD data reveals that, for all membranes and stoichiometries investigated, the variation in thickness is not proportional to water uptake. Upon increasing RH, film thickness h increases until reaching an asymptote, as shown in **Figure 3**(a), well described by $h=h_0(1-exp(-k\ RH))$, where k is a fitting parameter. Evidently, while increasing RH also increases water uptake, shown as a molar (and mass) ratio between water and polymer in **Figure 3**b, this behaviour is more complex. The correlation between water uptake and film swelling, shown in **Figure 3**c, is strikingly non-linear (and can be approximately fitted to an exponential).

In general, we find that increasing reaction time increases the thickness of both the dry and hydrated films, in approximately the same manner at all stoichiometries. Film thickness increases by approximately 2 nm in all cases (Figure S9). At fixed reaction time, increasing the concentration of MPD in the reaction, keeping TMC constant, correlates with reduced water uptake and swelling, as shown from a comparison between green (TMC/MPD 0.005/1%) and blue (0.005/0.1%) curves (**Figure 3**d-e). Under the same conditions, increasing the TMC concentration the variation in swelling is modest, while uptake increases considerably, visible by comparing the red (TMC/MPD 0.05/0.1%) and blue curves (**Figure 3**d-e). Generally, increasing reaction time decreases film water uptake, as well as swelling (measured as h/h_0), which is clearly shown with the blue (TMC/MPD 0.005/0.1 wt%) sets of data from light (1 min) to dark (20 min reaction time). Overall, **Figure 3**c establishes a broad proportionality between swelling and water uptake, which is unsurprising. However, at comparable swelling, the water uptake can vary significantly with reaction stoichiometry, as shown by the comparison with increasing TMC concentration, between blue (TMC/MPD 0.005/0.1 wt%) and red (0.05/0.1 wt%) curves and at 10 min in **Figure 3**c. All results are tabulated in detail in Supplementary Table S2. Overall, we find that upon increasing RH, the

11

membranes swell asymptotically and that even when film thickness no longer change considerably, water uptake continues, as highlighted by the non-linearity of **Figure 3**c.

Karode et al.[51] previously proposed that, at high reactant concentration in the organic phase, cluster polydispersity decreases with increasing reaction time, after passing through a maximum. In our results, a non-monotonic dependence of water uptake with reaction time is experimentally observed for the high TMC films (red, TMC/MPD 0.05/0.1 wt%) in **Figure 3**b. By comparison with membranes formed at lower TMC (cf. blue 0.005/0.1 wt% at 10 min), the mass densities and swelling are virtually identical, while the water uptake of the former is considerably higher (**Figures 3**d-e). Cluster polydispersity and association within the film have thus likely an impact in membrane response to water. Our data therefore suggest that tuning reaction stoichiometry and time, and presumably tuning PA membrane nanostructure, are effective strategies to control film swelling and water uptake (Figure S10).

To further rationalize the effect of reactant concentration on the film properties we focus on a fixed reaction time of 10 min in **Figure 4** and attempt to correlate data in terms of overall and partial densities. Overall, we have established above that increasing reaction time causes a densification of the membrane (detailed in Supplementary Table S2). For clarity, **Figure 4**a-c replots the dependence of water uptake and swelling at 10 min fixed reaction time, for the three stoichiometries. Significantly, we find that while water uptake follows an approximately linear dependence with RH, membrane swelling does not, saturating at high RH. Combined, we expect these to result in a non-monotonic change of density with RH, with an initial stage dominated by swelling, which is followed by further water uptake. We therefore compute the partial densities of the polymer ρ_{PA}, water ρ_{H2O}, as well as the total density ρ_{PA+H2O} as function of RH, in **Figures 4**d-f. The polymer partial density, **Figure 4**d, is computed from the initial polymer mass and film thickness h_0, upon swelling, i.e. from the measured h_{RH}. The total density, **Figure 4**f, was computed directly from the SLD dependence on RH, at fixed

12

polymer content, enabling the computation of the water partial density, **Figure 4**e. The lines are self-consistent, simultaneous fits to the data.

Films fabricated with the three stoichiometries evidently exhibit different responses to water. The largest swelling occurs upon initial exposure to water (low RH), while water uptake continues throughout the entire RH range. At the highest MPD concentration (1 wt%), the films exhibit the highest polymer density, as well as the lowest swelling and water uptake (Table S2). Increasing TMC concentration, at fixed MPD, however, is not found to affect the dry polymer density nor its response to RH (Table S2). However, the corresponding water uptake changes markedly. While ρ_{H2O} increases approximately linearly for the blue and green data, corresponding to lower TMC concentration (0.005 wt%), it is clearly non-monotonic for the red dataset (TMC 0.05 wt%), which has also the highest water uptake. The overall density of the latter reaches a plateau between 30 to 60% RH before increasing further up to 100% RH.

We hypothesise that a higher water uptake might be correlated to a 'looser' internal structure in the swollen state, derived from the oligomer formation and cluster organisation kinetics into a 'coherent' film and the overall non-linear film thickness evolution. The higher TMC concentration (red dataset) yields films of comparable thickness and density to those of lower TMC (blue dataset) at constant MPD, yet considerable larger water uptake. While the overall film thickness evolution with reaction time is similar in the two cases, the initial reaction kinetics is likely faster at high TMC, which is also compatible with highest h_0 at 1 min (Table S1). Faster initial kinetics could thus yield a more 'open' structure; however the two densities are effectively identical, which implies that pore structure and connectivity is likely responsible for the difference. By contrast, increasing MPD (green dataset) yields much thicker films, at comparable reaction times, but also denser and therefore with lower swelling and water uptake.

13

We next seek to correlate the detailed structural analysis reported so far, and its response to hydration, with RO membrane performance, in terms of permeance and salt rejection (**Figure 5**). Representative thin film membranes, at 10 min reaction time, were evaluated under cross-flow filtration at 20 bar and 2 g L^{-1} NaCl conditions for 100 h. All performance and structural parameters are given in Supplementary Table S3 (Figure S11).We find that the highest permeance is obtained for the membrane films which swell and uptakes most water and have the lowest density (red dataset, with highest TMC wt%). On the other hand, membranes with similar TMC concentration, but different MPD (blue and green datasets), albeit with very different membrane thickness, exhibit similar permeance (and water uptake), as shown in **Figure 5**a. By contrast, the highest salt rejection is obtained at low TMC and lower MPD concentrations, as shown in **Figure 5**b.Based on the findings reported in **Figure 4**, we find a clear dependence between permeance (or flux) and the water density within the membrane ρ_{H2O} at full hydration, as shown in **Figure 5**c. Salt rejection, on the other hand, is found to correlate favourably with the inverse of the total hydrated membrane density.

Employing AFM and FT-IR, Draževič *et al.*[54] investigated correlations between the swelling of commercial fully and partially aromatic polyamide membranes, as well as poly vinyl alcohol and cellulose acetate films, with water permeability. Despite scatter in the data, a positive correlation between permeability and swelling is found, as well as decrease in salt rejection, rationalized in terms of polymer rigidity and crosslinking. A similar trend has been proposed by *Freger et al.*[34] based on polyamide nanofiltration membranes subjected to an acid treatment and reported an increase in flux (and decrease of glucose rejection) with membrane swelling. In this case, a decrease in cross-linking was induced by the acid treatment. Separately, *Khorshidi et al.*[25] established that reducing the temperature of the organic phase yields thinner and smoother PA films with a greater degree of cross-linking and higher water flux. However, the reactant concentration employed (TMC/MPD 0.2/2 wt%) differs considerably from the much lower range 0.005-0.05/0.1-1 wt% employed in this work,

WILEY-VCH

preventing a direct comparison, as the network formation is expected to depend significantly on MPD diffusivity in the reaction zone.[25]

Somewhat surprisingly, no simple correlation is found between permeance and membrane swelling (Figure S11); we should note, however, that our structural measurements are carried out in the absence of applied pressure and water flux, while the performance data is obtained, evidently, under operating conditions. Moreover, the comparison is made between membranes of distinct reactant stoichiometry and well-defined thin films (with similar degree of cross-linking) in their pristine state. Indeed, when comparing membranes at fixed TMC (blue and green points) or MPD (blue and red points) concentration, a linear correlation between membrane permeance and swelling holds. This observation suggests that the IP mechanism and kinetics are fundamentally affected by reaction stoichiometry during film formation, resulting in different network and aggregate pore structure between those specimens. Salt rejection measurements corroborate this assertion. While the membrane with `looser` internal structure (red points) exhibits the lower salt rejection (≈69 %), membranes with similar dry density and membrane swelling (blue and red points) exhibit great differences in rejection (94 *vs* 69%); this latter is most likely due to the pore structure and connectivity, likely associated with different kinetics of film formation.

Our data indicate that higher permeance is obtained for stoichiometries exhibiting higher film swelling and water uptake and lower dry mass density. We tentatively interpret these results as due to differences in pore size, shape and connectivity, which are not directly probed by these experiments, derived from network and aggregate properties that evolve during the non-linear IP process.

3. Conclusion

Employing a recently developed synthetic route,[46] we investigate fully aromatic planar PA thin film membranes, obtained under highly controlled IP conditions, with

uniform thickness, of the order of 10 nm, and sub-nm roughness, over large surface areas (in excess of cm^2). These films can thus be investigated by neutron and X-ray reflectivity, providing unprecedented insight into the membrane structure at sub-nm spatial resolution along the direction normal to the surface (z), and statistically averaged across the plane of the film (xy) in a representative manner. This structural resolution also permits direct comparisons with theory and computer simulations of IP, allowing quantitative insight into the network formation mechanism and response to water, at the molecular level. We establish for the first time that PA thin films are compositionally homogeneous, on average, along the direction normal to the film surface in both dry and hydrated states. Possible compositional heterogeneity (related to surface polarisation effects) at either interface must thus be limited to < 1 nm in depth, i.e. commensurate with the interfacial width below which the ability to discriminate between composition and surface roughness is lost.

The evolution of film thickness with reaction time, at all stoichiometries investigated, can be described by a linear dependence within the 1-20 min range, but exhibit a markedly non-zero intercept. Since shorter reaction times do not result in robust membrane films (at these concentrations), we expect this stage to correspond to oligomerisation, cluster formation and aggregation, beyond which 'coherent' film are formed and grow. Our longest reaction times evidently do not reach the expected growth asymptote, and the measurement provides quantification of the initial to intermediate growth kinetics. Overall, our results clearly corroborate the mathematical approaches so far presented to model the reaction mechanism.

Different TMC/MPD stoichiometries, however, result in different growth kinetics and well as a range of physical properties, including film swelling and water uptake. We find that while water uptake is broadly proportional to film swelling, this relationship is highly non-linear, and can be generally described by an exponential dependence. Increasing TMC concentration

in the reaction is found to correlate with higher membrane swelling as well as higher water uptake. Increasing MPD concentration, on the other hand, broadly correlates with increasing film thickness and density, within the range investigated. As expected, increasing density decreases the swelling ability in water. The different reaction stoichiometries evidently impact the network formation mechanism and kinetics and thus RO performance, and full 3D structural resolution at sub-nm scale would be required to establish pore network geometry and connectivity, beyond the current 1D measurements. Our data provide unique insight into the relation between reaction conditions (stoichiometry and time), structure and performance relation of the PA active layer of RO membranes contributing towards the development of quantitative IP models and improved membrane separations.

4. Experimental Section

Membrane fabrication: Fully aromatic PA films were fabricated by interfacial polymerization of MPD and TMC at a water-hexane interface onto a sacrificial $Cd(OH)_2$ nanostrand layer supported by an ultrafiltration membrane, following a procedure reported previously.[46,55] Trimesoyl chloride (TMC) 98% and m-phenylenediamine (MPD) flakes 99+% were purchased from Sigma-Aldrich (Gillingham, UK). Polyimide polymer (P84) was purchased from HP Polymer GmbH (Austria), and cadmium chloride hydrate, Puratronic®, (99.998%) from Alfa Aesar, UK. Spectroscopic grade solvents (VWR International) and deionized water (Millipore) at 18 MΩ cm residual specific resistance were employed. Interfacial polymerization onto a Cd nanostrand support, with various reaction stoichiometries and reaction times as carried out, following a procedure reported earlier.[55] Solution concentrations are provided in terms of mass fraction of MPD in water, and TMC in hexane. Specifically, the nanostrand/PSf support layer was first soaked in 25 mL aqueous solutions of 0.1 or 1 wt% MPD. Film formation was then initiated by pouring 25 mL of the organic solution TMC in hexane at 0.005 or 0.05 wt%. Reaction times of 1, 10 and 20 min were

investigated. To enhance neutron reflection contrast, selected membranes were synthesized with deuterated MPD, *d4*-MPD (Toronto Research Chemicals, Canada). The resulting films were finally cleaned with hexane to remove any unreacted TMC. The sacrificial $Cd(OH)_2$ nanostrand layer was then removed by dissolution in water acidified to pH<5 with HCl, resulting also in the detachment of the PSf layer. The floated PA membrane films were then transferred to 3 inch, 275 μm Si(100) wafers (Si-Mat, Landsberg/Lech, Germany) for analysis. The SiO_x supports were cleaned by successive ultrasonication in acetone, ethanol and methanol followed by a final UV-O_3 treatment.

Neutron and X-ray reflectivity: Specular neutron reflectivity (NR) experiments were performed at the D17 reflectometer at the Institut Laue Langevin (Grenoble, France)[56] at angles 0.5 and 3.0, covering a momentum transfer normal to the surface ($Q_z=(4\pi/\lambda)sin\theta$) ranging from 0.006–0.3 Å^{-1}. A collimating slit geometry was used such that full use could be made of the coherent summing method for processing the data,[57] maximizing intensity without loss of resolution for the potentially non-flat samples during time-resolved measurements. An aluminium humidity chamber was employed to probe membrane swelling in-situ, within 0-100% relative humidity (RH), using heavy water D_2O (>99.7% D, Goss Scientific, UK) to enhance neutron contrast. Experiments were performed at fixed RH and continually cycling RH, as detailed in Supplementary Information. Complementary X-ray reflectivity (XRR) experiments were carried out with a PANalytical X'Pert PRO MPD diffractometer/reflectometer equipped with a Cu W/Si parabolic mirror (2.2 kW; λ=1.54 Å), beam attenuator (Ni 0.125 mm) and plate collimator (0.09°), 40 kV generator power and 40 mA, yielding a similar Q_z range of 0.01–0.3 Å^{-1}. Reflectivity profiles were analysed by the Abeles method using Motofit[58] and RasCAL,[59] enabling simultaneous, self-consistent analysis of datasets.

Membrane performance: A cross-flow filtration cell with a footprint of 0.001385 m^2 was operated with a steam of 100 L h^{-1} containing 2 g L^{-1} NaCl in water, at a temperature of

30° C and pressure of 20 bar. Transport data were measured at after 100 h, to ensure steady

state conditions.

Supporting Information
Supporting Information is available from the Wiley Online Library or from the author.

[1]   *ORNL. Materials for Separation Technologies: Energy & Emission Reduction*

        Opportunities 2005, DOI:10.2172/1218755.

[2]   L. F. Greenlee, D. F. Lawler, B. D. Freeman, B. Marrot, P. Moulin, *Water Res.* 2009,

        43, 2317.

[3]   W. J. Koros, R. P. Lively, *AIChE J.* 2012, **58**, 2624.

[4]   R. W. Baker, *Membrane Technology and Applications, 3rd Edition*, John Wiley &

        Sons, Ltd, Chichester, UK, **2012**.

[5]   A. K. Pabby, S.S.H. Rizvi and A.M.S. Requena, *Handbook of membrane separations:*

        Chemical, Pharmaceutical, Food and Biotechnological applications, 2nd Editions,

        CRC press, Taylor & Francis group, **2015**.

[6]   W. J. Lau, A. F. Ismali, N. Misdan, M. A. Kassim, *Desalination,* 2012, **287**, 190.

[7]   C. Fritzmann, J. Löwenberg, T. Wintgens, T. Malin, *Desalination*, 2007, **216**, 1.

[8]   S. S. Shenvi, A. M. Isloor, A. F. Ismail, *Desalination* 2015, **368**, 10.

[9]   M. M. Khin, A. S. Nair, V. J. Babu, R. Murugan, S. Ramakrishna, *Energy Environ. Sci.*

        2012, **5**, 8075.

[10]   R. J. Petersen, *J. Membr. Sci.* 1993, **83**, 81.

[11]   M. T. M. Pendergast, E. M. V. Hoek, *Energy Environ. Sci.* 2011, **4**, 1946.

[12]   D. Li, H. Wang, *J. Mater. Chem.* 2010, **20**, 4551.

[13]   S.-J. Kim, B. S. Oh, H.-W. Yu, L. H. Kim, C.-M. Kim, E.-T. Yang, M. S. Shin, A. Jang, M. H. Hwang, I. S. Kim, *Desalination* 2015, **370**, 44.

[14]   C. Sun, L. Xie, X. Li, L. Sun, H. Dai, *Desalination* 2015, **371**, 18.

[15]   D. Cohen-Tanugi, R. K. McGovern, S. H. Dave, J. H. Lienhard, J. C. Grossman, *Energy Environ. Sci.* 2014, **7**, 1134.

[16]   J. R. Weber, C. O. Osuji, M. Elimelech, *Nature Rew. Materials* 2016, **1**, 1.

[17]   H. B. PArk, J. Kamcev, L. M. Roberson, M. Elimelech, B. D. Freeman, *Science* 2017, **356**, 1137.

[18]   M. Mulder, *Basic principles of membrane technology, 2nd Edition*, Kluwer Academic Publisher, Springer, Netherlands, **1997**.

[19]   I. Pinnau and B. D. Freeman, *Membrane formation and modification*, ACS Symposium Series, American Chemical Society, Washington, DC, **1999**.

[20]   P. W. Morgan, *Condensation polymers: by interfacial and solution methods*, Interscience Publisher, John Wiley, New York, **1965**.

[21]   P. W. Morgan, S. L. Kwolek, *J. Polym. Sci. Part A Polym. Chem.* 1996, **34**, 531.

[22]   J. E. Cadotte, R. S. King, R. J. Majerle, R. J. Petersen, *J. Macromol. Sci. Part A – Chem.* 1981, **A15**, 727.

[23]   F. Pacheco, R. Sougrat, M. Reinhard, J. O. Leckie, I. Pinnau, *J. Membr. Sci.* 2016, **501**, 33.

[24]   A. K. Ghosh, B. H. Jeong, H. Huang, E. M. V. Hoek, *J. Membr. Sci.* 2008, **311**, 34.

[25]   B. Khorshidi, T. Thundat, B. A. Fleck, M. Sadrzadeh, *Sci. Rep.* 2016, **6**, 22069.

[26]   M. M. Klosowski, C. M. McGilvery, Y. Li, P. Abellan, Q. Ramasse, J. T. Cabral, A. G. Livingston, A. E. Porter, *J. Membr. Sci.* 2016, **520**, 465.

[27] X. Lu, S. Nejati, Y. Choo, C. O.Osuji, J. Ma, M. Elimelech, *Appl. Mater. Interfaces* 2015, **7**, 16917.

[28] V. Freger, *Langmuir* 2003, **19**, 4791.

[29] O. Coronell, B. J. Mariñas, D. G. Cahill, *Environ. Sci. Technol.* 2011, **45,** 4513.

[30] S.-Y. Kwak, S. C. Jung, S. H. Kim, *Environ. Sci. Technol.* 2001, **35**, 4334.

[31] D. G. Cahill, V. Freger, S.-Y. Kwak, *MRS Bull.* 2008, **33**, 27.

[32] B. Mi, O. Coronell, B. J. Mariñas, F. Watanabe, D. G. Cahill, I. Petrov, *J. Membr. Sci.* 2006, **282**, 71.

[33] Q. Li, X. Pan, C. Hou, Y. Jin, H. Dai, H. Wang, X. Zhao, X. Liu, *Desalination* 2012, **292**, 9.

[34] V. Freger, A. Bottino, G. Capannelli, M. Perry, V. Gitis, S. Belfer, *J. Membr. Sci.* 2005, **256**, 134.

[35] E. P. Chan, A. P. Young, J.-H. Lee, J. Y. Chung, C. M. Stafford, *J. Polym. Sci. B Polym. Phys.* 2013, **51,** 385.

[36] E. P. Chan, A. P. Young, J.-H. Lee, C. M. Stafford, *J. Polym. Sci. B Polym. Phys.* 2013, **51**, 1647.

[37] E. P. Chan, S. C. Lee, *J. Polym. Sci. B Polym. Phys.* 2017, **55**, 412.

[38] F. A. Pacheco, I. Pinnau, M. Reinhard, J. O. Leckie, *J. Membr. Sci.* 2010, **358**, 51.

[39] V. Kolev, V. Freger, *Polymer* 2014, **55,** 1420.

[40] J. Muscatello, E. A. Muller, A. A. Mostofi, A. P. Sutton, *J. Membr. Sci.* 2017, **527**, 180.

[41] M. Ding, A. Szymczyk, F. Goujon, A. Soldera, A. Ghoufi, *J. Membr. Sci.* 2014, **458**, 236.

[42] Y. Xiang, Y. Liu, B. Mi, Y. Leng, *Langmuir* 2013, **29**, 11600.

[43] E. Harder, D. E. Walters, Y. D. Bodnar, R. S. Faibish, B. Roux, *J. Phys. Chem. B,* 2009 **113**, 10177.

[44]   E. P. Chan, J. H. Lee, J. Y. Chung, C. M. Stafford, *Rev. Sci. Instrum.* 2012, **83,** 114102.

[45]   W. Choi, S. Jeon, S. J. Kwon, H. Park, Y.-I. Park, S.-E. Nam, P. S. Lee, J. S. Lee, J. Choi, S. Hong, E. P. Chan, J.-H. Lee, *J. Membr. Sci.* 2017, **527**, 121.

[46]   S. Karan, Z. Jiang, A. G. Livingston, *Science* 2015, **348**, 1347.

[47]   Y. Zhu, W. Xie, S. Gao, F. Zhang, W. Zhang, Z. Liu, J. Jin, *Small* 2016, **12**, 5034.

[48]   J.-J. Wang, H.-C. Yang, M.-B. Wu, X. Zhang, Z.-K. Xu, *J. Mater. Chem. A* 2017, DOI: 10.1039/C7TA00501F.

[49]   V. Freger, S. Srebnik, *J. Appl. Polym. Sci.* 2003, **88**, 1162.

[50]   R. Nadler S. Srebnik*, J. Membr. Sci.* 2008, **315**, 100.

[51]   S. K. Karode, S. S. Kulkarni, A. K. Suresh, R. A. Mashelkar*, Chem. Eng. Sci.* 1998, **53**, 2649.

[52]   K. Košutić, L. Kaštelan-Kunst, B. Kunst, *J. Membr. Sci.* 2000, **168**, 101.

[53]   S. H. Kim, S.-Y. Kwak, T. Suzuki, *Environ. Sci. Technol.* 2005, **39**, 1764.

[54]   E. Draževic, K. Košutić, V. Freger, *Water Res.* 2014, **49**, 444.

[55]   S. Karan, S. Samitsu, X. Peng, K. Kurashima, I. Ichinose, *Science* 2012, **335**, 444.

[56]   R. Cubitt, G. Fragneto, *Appl. Phys. A: Mater. Sci. Process.* 2002, **M** *74,* S329.

[57]   R. Cubitt, T. Saerbeck, R. A. Campbell, R. Barker, P. Gutfreund, *J. Appl. Crystallogr.* 2015, **48**, 2006.

[58]   A. J. Nelson, *J. Appl. Crystallogr.* 2006, **39**, 273.

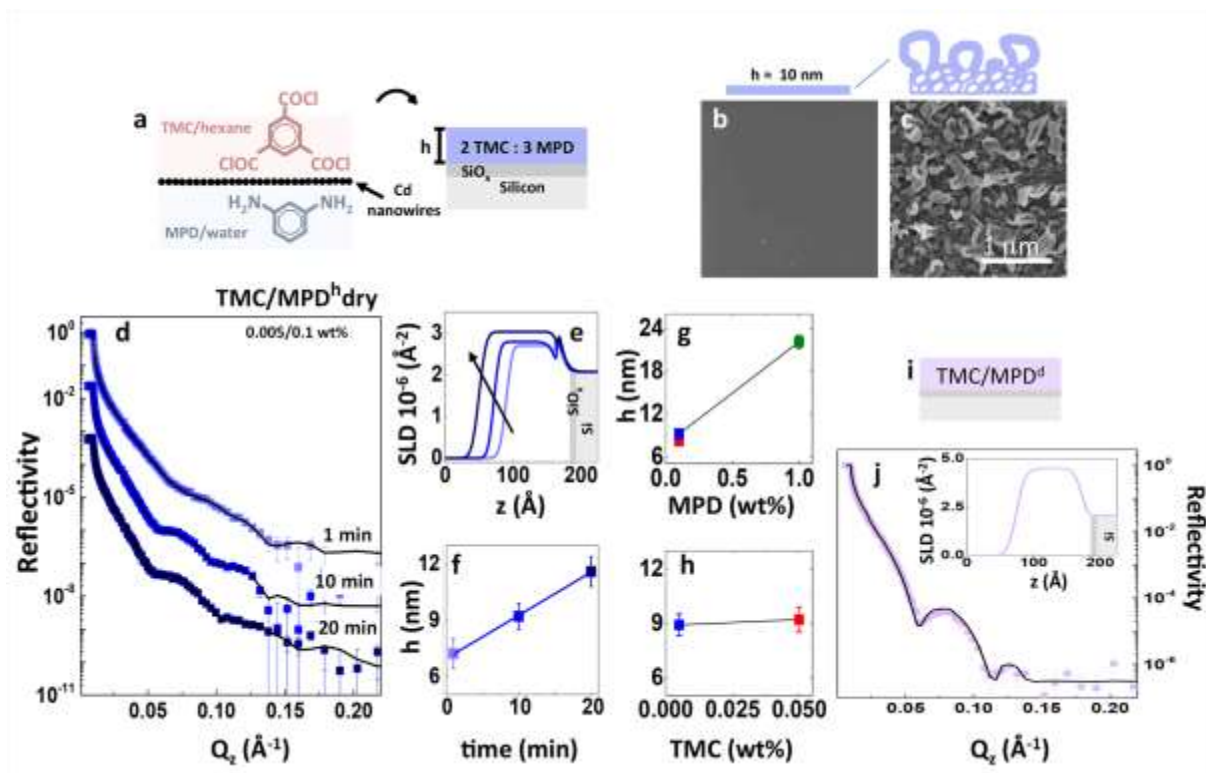[59]   RasCal: http://sourceforge.net/projects/rscl/, accessed: May, 2015.

Figure 1. a) Schematic of the interfacial polymerization (IP) reaction between TMC and MPD at the organic/water interface. Smooth, planar PA films with thickness *h* are transferred onto a Si/SiOx support for reflectivity. b) SEM picture of smooth nanofilm from TMC/MPD (0.005/0.1 wt%, 10 min reaction time) on polysulfone. c) SEM picture of crumpled nanofilm from TMC/MPD (0.15/3 wt%, 10 min reaction time) on polysulfone. d) NR data and model fits for dry TMC/MPD 0.005/0.1 wt% films obtained at reaction times 1, 10 and 20 min. e) Corresponding SLD profile, where *z* is the distance normal to the film surface. f) Film thickness *h* dependence on the reaction time. g) Variation of *h* with MPD concentration after 10 min reaction time, with TMC 0.005 (blue, green) and 0.05 (red) wt%. h) Variation of *h* with TMC concentration, with MPD 0.1 wt% (blue, red). i-j) NR of a representative TMC/MPD^d membrane with 0.005/0.1 wt% and reaction time 1 min (corresponding to the first membrane in panel d), and the SLD profile, shown to be uniform across membrane thickness.
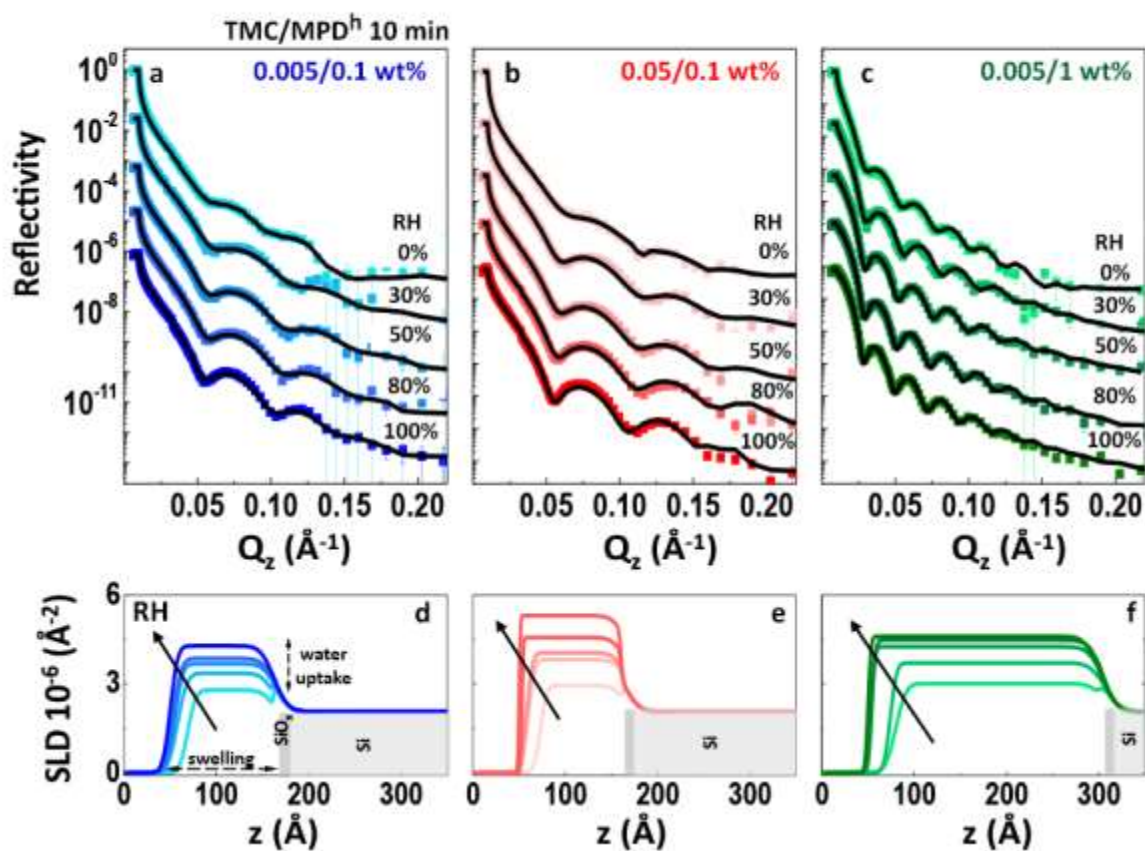
Figure 2. a-c) NR data and model fits for TMC/MPD 0.005/0.1; 0.05/0.1 0.005/1 wt% films obtained at reaction times 10 min. d-f) Corresponding SLD profiles, where *z* is the distance normal to the film surface. The arrows indicate the increase in SLD due to the heavy water uptake as consequence of the increasing in relative humidity.
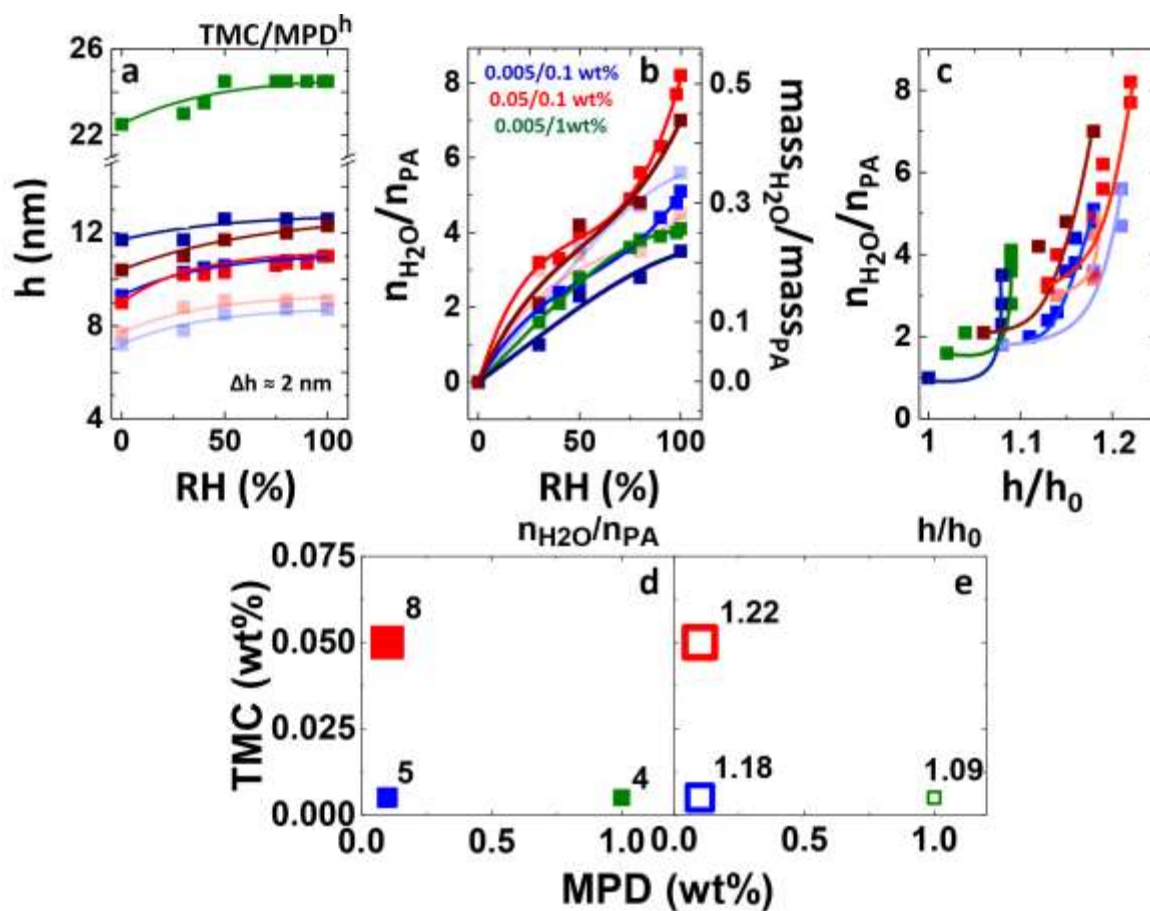
Figure 3. a) Variation of membrane thickness as function of relative humidity (lines are inverse exponential fits). b) Variation of water uptake as function of relative humidity (lines are guides to the eye). c) Variation of water uptake as function of membrane swelling. The comparison between the three investigated stoichiometries (TMC/MPD 0.005/0.1; 0.05/0.1 0.005/1 wt% thin films; blue, red and green curves, respectively) are reported for the entire range of reaction times investigated (1, 10 and 20 min; from light to darker colours, respectively (lines are guides to the eye). d-e) Water uptake and membrane swelling (panel d and e, respectively) as function of the reactant concentration at fixed reaction time (10 min).
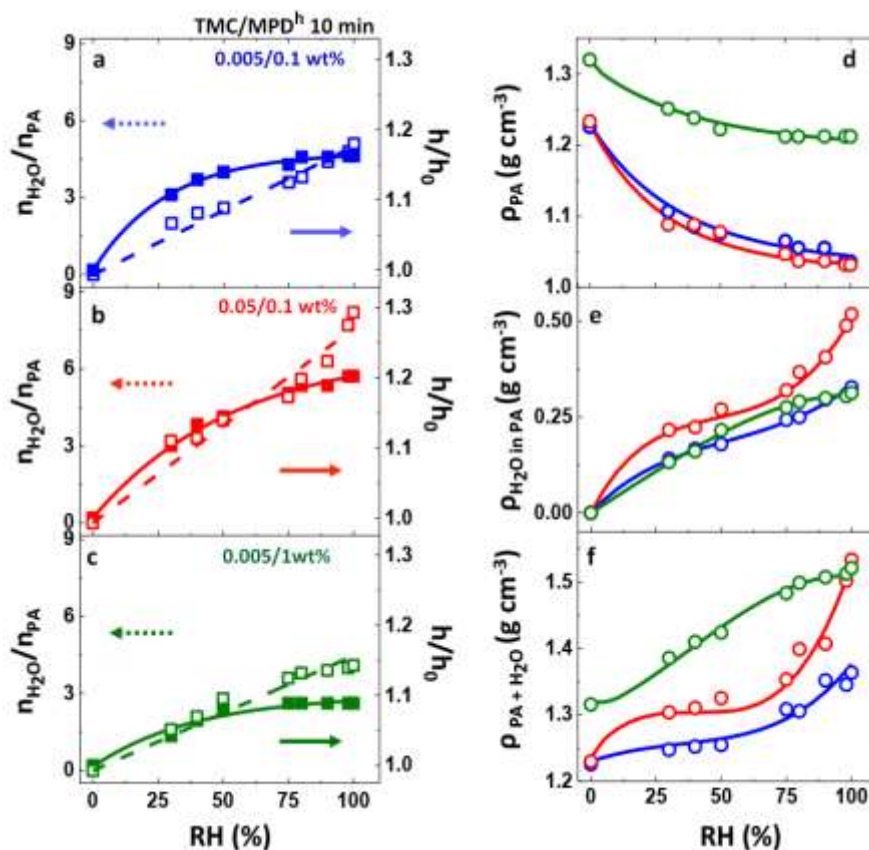
Figure 4. a) Variation of water uptake and membrane swelling as function of relative humidity for TMC/MPD 0.005/0.1 wt% thin film, at 10 min reaction time. b) Variation of water uptake and membrane swelling as function of relative humidity for TMC/MPD 0.05/0.1 wt% thin film at 10 min reaction time. c) Variation of water uptake and membrane swelling as function of relative humidity for TMC/MPD 0.005/1 wt% thin film at 10 min reaction time. d) Variation of polymer density as function of membrane swelling for the three thin film at 10 min reaction time (TMC/MPD 0.005/0.1; 0.05/0.1 0.005/1 wt%; blue, red and green curves, respectively). e) Variation of water density inside the membrane as function of membrane swelling for the three thin film at 10 min reaction time (TMC/MPD 0.005/0.1; 0.05/0.1 0.005/1 wt%; blue, red and green curves, respectively). f) Variation of membrane (polymer and water) density as function of membrane swelling for the three thin film at 10 min reaction time (TMC/MPD 0.005/0.1; 0.05/0.1 0.005/1 wt%; blue, red and green curves, respectively).
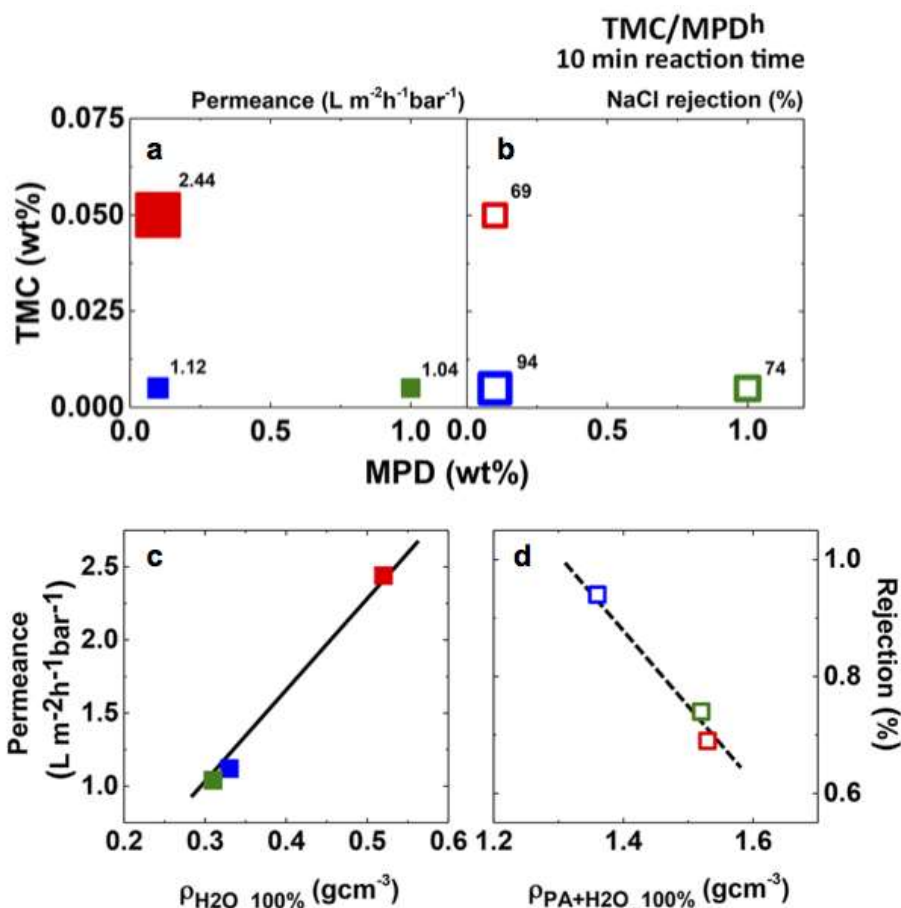
Figure 5. a-b) Variation of membrane permeance and NaCl rejection as function of reactant concentration at fixed reaction time (10 min). membrane swelling for the three thin films at 10 min reaction time (TMC/MPD 0.005/0.1; 0.05/0.1 0.005/1 wt%; blue, red and green curves, respectively). c) Variation of membrane permeance as function of water partial density (at 100% RH) for the three thin films at 10 min reaction time (TMC/MPD 0.005/0.1; 0.05/0.1 0.005/1 wt%; blue, red and green points, respectively). d) Variation of NaCl rejection as function of total density (at 199% RH) for the three thin films at 10 min reaction time (TMC/MPD 0.005/0.1; 0.05/0.1 0.005/1 wt%; blue, red and green points, respectively).

Supporting Information

Neutron reflectivity and performance of polyamide nanofilms for water desalination

Fabrizia Foglia, Santanu Karan, Manuela Nania, Zhiwei Jiang, Alexandra E. Porter, Robert Barker, Andrew G. Livingston, João T. Cabral*

Table of Contents

Thin film preparation:

Polyamide thin films were prepared by interfacial polymerisation (IP). IP is a polycondensation between two multifunctional monomers dissolved in immiscible solvents (formally an aqueous and an organic phase), which takes place at the interface between the two solvents. Formally the organic-soluble component (acid chloride) is insoluble into the polymer, whereas the water-soluble component (an aromatic amine, formally *m*-phenylenediamine, MPD) diffuses through the film to react with the acid chloride (trimesoyl chloride, TMC) at the film/organic phase interface, where the film grows.

Membranes obtained via IP, including commercial RO membranes, are highly inhomogeneous (Figure S1a-c) in terms of spatial variation, chemistry and porosity.[1-2] This intrinsic heterogeneity makes structural characterization of the folded skin layer, of the order of 10 nm in thickness, challenging. Recently, a controlled synthetic route has been developed by *Karan et al.*,[3] yielding ultrathin, planar, films supported by Cd-nanowires. These can now be transferred onto other supports (e.g. silicon wafer used in reflectivity of neutrons and X-rays) for detailed structural investigations (Figure S1d-h). This paper reports the first reflectivity studies benefitting from the advent of this synthetic route.
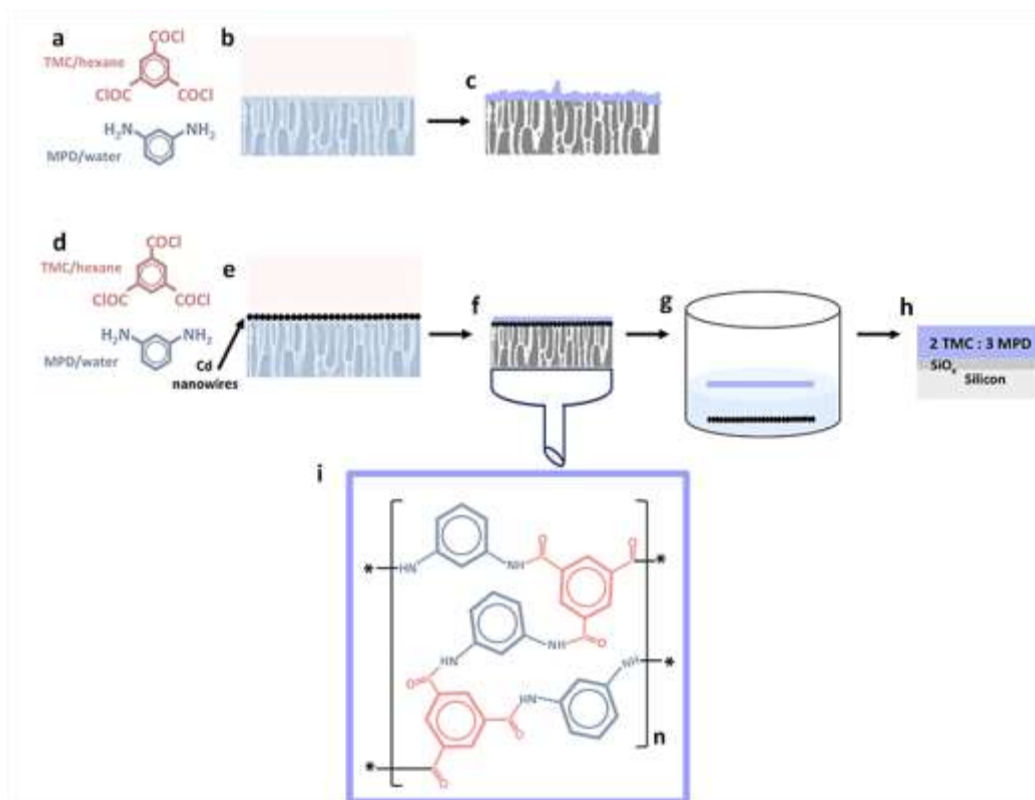
Figure S1. a-c) Cross-sectional view of conventional IP and resulting membranes, generally supported by a polysulfone layer and polyester backing. d-e) Controlled IP onto Cd nanostrands. f-h) Schematic of the fabrication of the free-standing nanofilm and its transfer onto a silicon wafer, by dissolution of the nanowires with an aqueous solution at pH< 5 (panel g) and film floating. i) Schematic of a planar cross-linked PA polymer film (TMC/MPD 2:3) supported by a Si/SiO$_x$ wafer.

Neutron reflectivity:

Reflectivity measurements were carried out at D17 (ILL, Grenoble) and SURF (ISIS, Oxfordshire) and data were analysed using conventional software packages RasCAL[4] and MOTOFIT.[5] For clarity, the extraction of quantitative composition data from fitted scattering length density (SLD) measurements is detailed below.

For all stoichiometries, the dry films were analysed initially and the dry thickness h_0 and interfacial roughness estimated. A single layer model was found to describe all NR data.

In atomic terms, $SLD = \Sigma_i b_i / V$, $[cm^{-2}]$ corresponding to the sum of the scattering length of all atoms i, in sample volume V. In molar terms, the SLD of a dry membrane film reads:

$$SLD_{dry} = (n_{PA}/A)\ (N_A b_{PA})/(h_0) \tag{S1}$$

where n_{PA} is the number of moles of PA unit in the sample volume, written as $V = A\ h_0$, where A is the sample footprint (illuminated area) and h_0 is the sample thickness. The value of b_{PA} can be calculated from the chemical structure repeat unit of the polymer network, taken to be $C_{18}H_{12}O_3N_3$, which corresponds to a ratio of 1 TMC:1.5 MPD which is known to apply for fully crosslinked PA films.[1,3] We have thus used $b_{PA} = 120.24\ 10^{-13}$ cm. Since h_0 is measured independently, the value of n_{PA}/A can thus be readily determined, corresponding to the number of moles of PA units over the measured footprint.

Thin films exhibit intrinsic surface roughness which manifests itself in NR data by 'rounding' the SLD profiles, as illustrated in Figure S2. During NR data fitting, this interfacial profile is modelled considering a series of thin layers with SLD related by a given profile (eg hyperbolic tangent), ranging down to SLD = 0, corresponding to air, or the SLD on the support layers (e.g. SiOx). This intrinsic interfacial width between layers or roughness (air interface) sets a finite resolution for detecting minute composition (or density) differences at the film interfaces. In all data reported, the

surface roughness is no larger than 1 nm, setting an upper limit for any asymmetry in compositional profile of the PA layer along the direction normal to the film surface. As mentioned in the main text, reflectivity measurements yield averages overall a large footprint of cm^2, and thus infrequent, local variations along the plane (xy) become inconsequent for the final result. By contrast, a statistically significant measurement with exceptional resolution (A) is obtained along the z-direction.
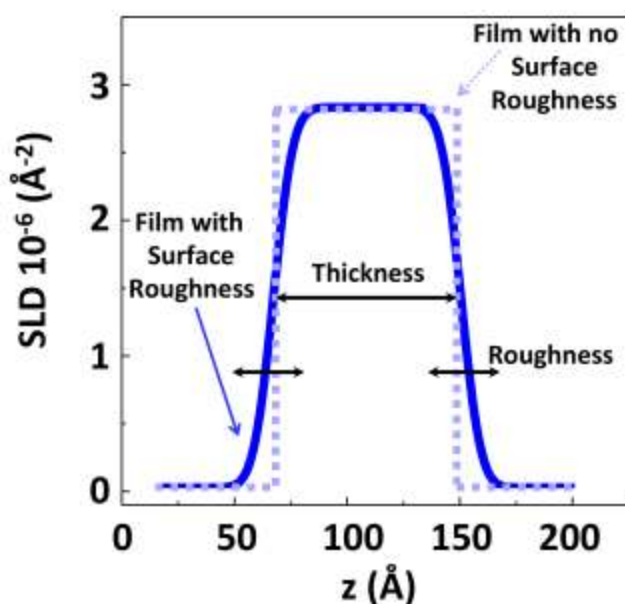

Figure S2. Schematic of a SLD profile in which are highlighted thickness and surface roughness. In the plot are compared SLD profiles for and ideal and real sample having same layer thickness. The ideal profile corresponds to a roughness-free sample (dash line); the real sample is the one with a no-zero surface roughness (solid line).

Upon hydration, the NR data remain well described by a single layer, whose SLD value as well as film thickness depend on RH, termed SLD_{RH} and h_{RH}. While the latter is directly determined by data fitting, the SLD of the hydrated polymer layer can de interpreted as:

$$SLD_{RH} = (n_{PA} N_A b_{PA})/(h_{RH} A) + (n_{D2O} N_A b_{D2O})/(h_{RH} A) \qquad (S2)$$

where n_{D2O} is now the number of moles of (heavy) water and b_{D2O} is its scattering length 19.14 10^{-13} cm. Evidently, the polymer content remains fixed upon hydration

and the only unknown of Eq. (S2) is n_{D2O}/A. The water uptake can be readily determined as the ratio between $(n_{D2O}/A)/(n_{PA}/A) = n_{D2O}/n_{PA}$ and A is thus implicit in our analysis.

The dry polymer density is readily calculated from

$$\rho_{TOT(RH)} = (n_{PA}/A)\,(M_{w\_PA}/h_0) \tag{S3}$$

where M_{w_PA} is molecular weight of a PA unit (318 g mol^{-1}). Upon hydration, the total membrane density (including PA and heavy water) reads:

$$\rho_{PA+D2O} = ((n_{PA}M_{w\_PA})+(n_{D2O}M_{w\_D2O}))/(h_{RH}\,A) \tag{S4}$$

which can be calculated from the analysis above, as well as the partial densities:

$$\rho_{PA} = (n_{PA}M_{w(PA)})/(h_{RH}\,A) \tag{S5}$$

$$\rho_{D2O\_in\_PA} = (n_{D2O}M_{w(D2O)})/(h_{RH}\,A) \tag{S6}$$

For clarity, we have termed heavy water by H_2O in the figures of the main paper.

Reflectivity experiments were performed at fixed RH values (0, 30 and 100% RH) and continually increasing RH from 30 to 100%. In order to establish the reversibility of the process some samples have also been dehydrated *in situ*. The 0% RH condition was attained by adding silica gel into the humidity chamber; on the other hand the RH range between 30 to 100% has been achieved by independently controlling the sample and water reservoir temperature. Specifically, the water reservoir generates saturated vapour pressure when its temperature, T_w, is lower or equal to the sample temperature, T_s. In our case, each RH% was achieved by keeping fixed the sample temperature (25° C) and increasing the temperature of the water reservoir in a range between (5° and 25° C).
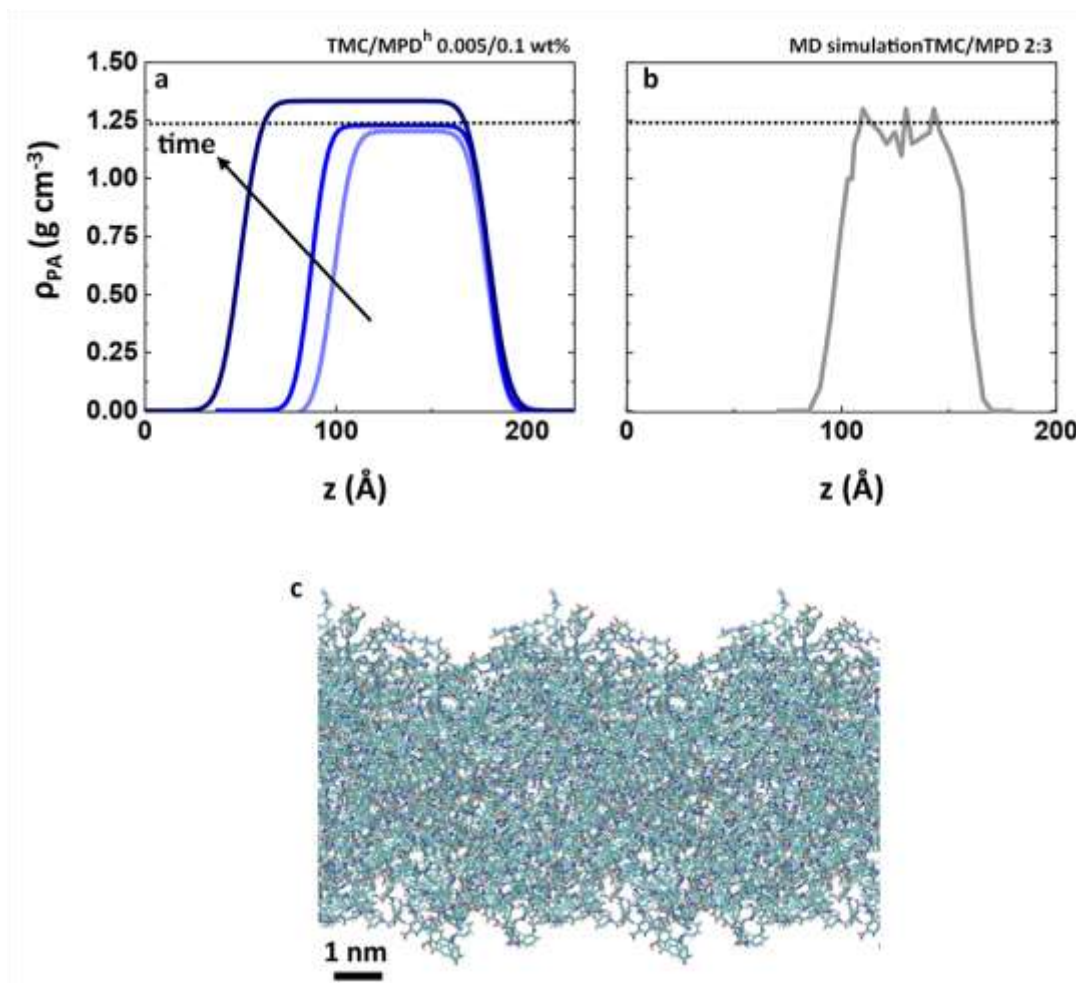
Figure S3. a) Density profile for TMC/MPD 0.005/0.1 wt% thin films obtained at reaction times 1, 10 and 20 min. b) Density profile for TMC/MPD 2:3 obtained via molecular dynamics simulation. c) Molecular dynamics simulation for TMC/MPD 2:3 thin film.

Our experimentally measured density can be compared with recent molecular dynamics simulations of interfacial polymerisation.[6] These MD results are particularly significant since based on the experimental procedure for polyamide (PA) film synthesis, starting with MPD and TMC initially separated by an interface, and yielding PA films with the correct TMC/MPD 2:3 stoichiometry and with realistic bond distances obtained from density functional theory (DFT). The authors find that the interfacial polymerization reaction proceeds by reaction and diffusion of MPD into the organic, TMC-rich phase, resulting in the formation of clusters and then cluster aggregates, finally spanning a PA film.[6-8] As reported by several authors, the reaction was found to be 'self-limiting' upon percolation and thin film formation, hinders further permeation of MPD (or TMC) across the interface. The simulated

34

membranes display a thickness of 5-10 nm in broad agreement with our findings, and a surface roughness of 1-4 nm. The latter is higher than the roughness revealed by NR (and XR) which is likely due to the small simulation box size (viz 50 nm) by contrast with the measured surface area of several cm^2. The simulated and measured densities, shown in Figure S3a-b are in remarkably good agreement, and the film structure at a high MPD:TMC ratios provides a useful visual representation of the membrane structure. Possible local spatial heterogeneities within the film structure cannot be resolved, since reflectivity measurements yield high resolution average SLD profiles *normal* to the membrane surface (1D).

Some MD simulations suggest a degree of compositional heterogeneity at both membrane interfaces, associated with surface polarization for these FT-30 type of films.[6,8-11] Our SLD profiles do not support the suggestion of a large surface layer, i.e. wider than the measured interfacial width of <1 nm. This value can be taken as an upper limit, therefore, for compositional segregation. Specifically, considering the SLD of trimesic acid (3.4x10^{-6} Å^{-2}; $C_9H_6O_6$ and 4x10^{-6} Å^{-2}; when fully deprotonated $C_9H_3O_6^{3-}$), the absence of a sharp signal with SLD around 3.7x10^{-6} Å^{-2} can only be compatible with a skin thickness of up to a few Ångstroms.

Reactant concentration and reaction time dependence:

Using Karan's synthetic pathway[3] we produced a series of fully cross-linked polymeric nanofilm as a function of reactant stoichiometry and reaction time. More specifically we investigated 3 stoichiometries, namely TMC/MPD 0.005/0.1 (blue points), 0.05/0.1 (red points) and 0.005/1 wt% (green points), allowing the reaction to continue from 1 up to 20 min (namely 1, 10 and 20 min).

The comparison between the three investigated stoichiometries, at constant reaction time (10 min), indicates that the concentration of MPD in the reaction batch determines the final thin film thickness (Figure S4). The latter is compatible with MPD

acting as limiting factor for the reaction, and is expected from the self-limiting nature of IP.[12] Another feature emerging by comparing different stoichiometries at fixed reaction time is the slight increase in surface roughness with the increase of MDP concentration in the reaction batch. The latter is likely due to the cluster aggregation process[9] where the bond formation between unreacted side groups on the cluster surface becomes sterically hindered.[6]
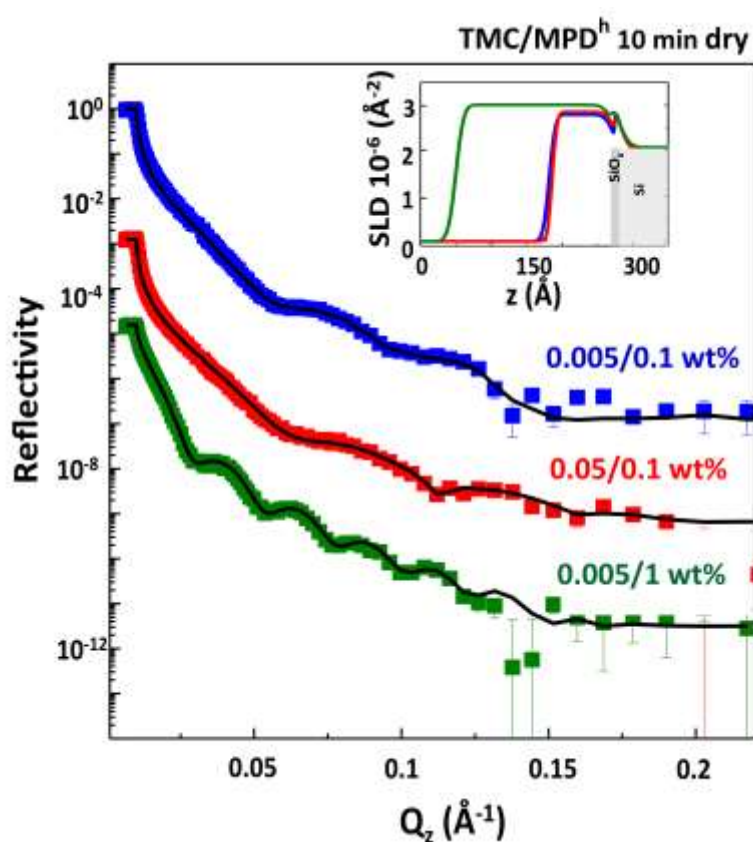

Figure S4. NR data and model fits for dry TMC/MPD films obtained at 10 min reaction times for the stoichiometries 0.005/0.1; 0.05/0.1 and 0.005/1 wt% (blue, red and green curves, respectively). In the inset are reported the corresponding SLD profiles, where z is the distance normal to the film surface.

It is interesting to notice that, regardless of the reactant stoichiometry, the thin films have similar chemical structure and mass density, which increases with the reaction

time (Tables S1 and S2). Furthermore, also in the case of high TMC concentration (Figure S5), the analysis indicates a linear dependence, with no zero intercept, between membrane thickness and reaction time. Within the time window probed, the film thickness grows as *h = 0.13 t + 7.82*, where *h* is film thickness in nm, and *t* is reaction time in min, at this reagent stoichiometry (Tables S1 and S2). Remarkably, at these experimental conditions, the film formation seems to follow a different kinetics (slower; slope = 0.13 *vs* 0.24 for TMC/MPD 0.05/0.1 and 0.005/0.1, respectively) and it results thicker within a certain range (77 *vs* 72 Å for films obtained at 1 min reaction time, TMC/MPD 0.05/0.1 and 0.005/0.1, respectively). This is associated to the diffusion rate of MPD across the already formed highly cross-linked film as consequence of the "self-limiting" nature of the process as well as the nucleation rate.[10,13]
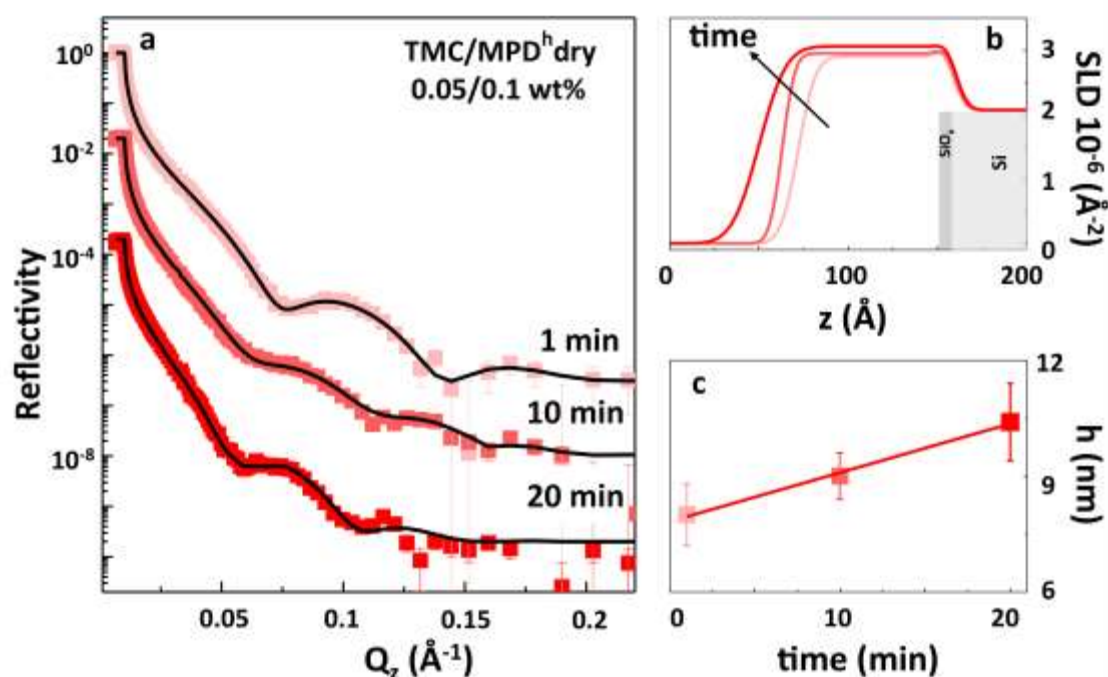

Figure S5. a) NR data and model fits for dry TMC/MPD 0.05/0.1 wt% films obtained at reaction times 1, 10 and 20 min. b) Corresponding SLD profile, where z is the distance normal to the film surface. c) Film thickness *h* dependence on reaction time.

Table S1. Results of simultaneous model fits to NR data at different relative humidity percentages. In the table are reported: thickness, roughness and SLD for all investigated thin films.

Sample	Parameter	0% RH	30% RH	50% RH	80% RH	100% RH
TMC/MPD[h]	Thickness (Å)	72 ± 2	78 ± 1	85 ± 2	87 ± 2	87 ± 1
0.005/0.1 w t%	Roughness (Å)	8 ± 1	7 ± 1	5 ± 1	5 ± 2	4 ± 1
1 min time	SLD 10^{-6} (Å^{-2})	2.77 ± 0.05	3.27 ± 0.05	3.66 ± 0.05	3.98 ± 0.05	4.31 ± 0.05
TMC/MPD[h]	Thickness (Å)	93 ± 2	103 ± 1	106 ± 1	109 ± 1	109 ± 1
0.005/0.1 w t%	Roughness (Å)	7 ± 1	8 ± 1	7 ± 1	7 ± 1	6 ± 1
10 min time	SLD 10^{-6} (Å^{-2})	2.79 ± 0.05	3.34 ± 0.05	3.67 ± 0.05	3.85 ± 0.05	4.28 ± 0.05
TMC/MPD[h]	Thickness (Å)	117 ± 2	117 ± 2	126 ± 1	126 ± 1	126 ± 1
0.005/0.1 w t%	Roughness (Å)	8 ± 1	8 ± 1	6 ± 1	7 ± 1	6 ± 1
20 min time	SLD 10^{-6} (Å^{-2})	3.03 ± 0.05	3.13 ± 0.05	3.86 ± 0.05	3.86 ± 0.05	4.39 ± 0.05
TMC/MPD[h]	Thickness (Å)	77 ± 1	88 ± 2	91 ± 2	91 ± 1	91 ± 1
0.05/0.1 w t%	Roughness (Å)	8 ± 1	7 ± 1	7 ± 2	6 ± 2	7 ± 1
1 min time	SLD 10^{-6} (Å^{-2})	2.79 ± 0.05	3.61 ± 0.05	3.64 ± 0.05	3.68 ± 0.05	4.04 ± 0.05
TMC/MPD[h]	Thickness (Å)	90 ± 1	102 ± 1	103 ± 1	108 ± 1	109 ± 1
0.05/0.1 w t%	Roughness (Å)	8 ± 1	7 ± 1	7 ± 1	5 ± 2	5 ± 1
10 min time	SLD 10^{-6} (Å^{-2})	2.80 ± 0.05	3.79 ± 0.05	4.02 ± 0.05	4.53 ± 0.05	5.28 ± 0.05
TMC/MPD[h]	Thickness (Å)	104 ± 2	110 ± 2	117 ± 2	120 ± 1	123 ± 1
0.05/0.1 w t%	Roughness (Å)	10 ± 1	10 ± 2	9 ± 1	7 ± 1	7 ± 1
20 min time	SLD 10^{-6} (Å^{-2})	2.86 ± 0.05	3.63 ± 0.05	4.25 ± 0.05	4.39 ± 0.05	5.13 ± 0.05
TMC/MPD[h]	Thickness (Å)	225 ± 1	230 ± 2	244 ± 1	245 ± 1	245 ± 1
0.005/1 w t%	Roughness (Å)	9 ± 1	5 ± 2	5 ± 1	5 ± 1	5 ± 1
10 min time	SLD 10^{-6} (Å^{-2})	3.00 ± 0.05	3.74 ± 0.05	4.22 ± 0.05	4.49 ± 0.05	4.56 ± 0.05

Table S2. Results of simultaneous model fits to NR data at different relative humidity percentages. In the table are reported: water uptake (n_{H2O}/n_{PA}), mass density (ρ_{PA+H2O}) and membrane swelling for all investigated thin films.

Sample	Parameter	0% RH	30% RH	50% RH	80% RH	100% RH
TMC/MPD[h]	n_{H2O}/n_{PA}	0	2	4	5	6
0.005/0.1 wt%	ρ_{PA+H2O} (gcm^{-3})	1.21	1.24	1.26	1.30	1.35
1 min time	Swelling (%)	0	8	18	21	21
TMC/MPD[h]	n_{H2O}/n_{PA}	0	2	3	4	5
0.005/0.1 wt%	ρ_{PA+H2O} (gcm^{-3})	1.23	1.25	1.25	1.31	1.37
10 min time	Swelling (%)	0	11	13	16	18
TMC/MPD[h]	n_{H2O}/n_{PA}	0	2	2	2	3
0.005/0.1 wt%	ρ_{PA+H2O} (gcm^{-3})	1.33	1.35	1.42	1.42	1.51
20 min time	Swelling (%)	0	0	8	8	8
TMC/MPD[h]	n_{H2O}/n_{PA}	0	3	3	3	3
0.05/0.1 wt%	ρ_{PA+H2O} (gcm^{-3})	1.22	1.28	1.26	1.27	1.33
1 min time	Swelling (%)	0	14	18	18	18
TMC/MPD[h]	n_{H2O}/n_{PA}	0	3	4	6	8
0.05/0.1 wt%	ρ_{TOT} (gcm^{-3})	1.23	1.30	1.35	1.40	1.53
10 min time	Swelling (%)	0	13	14	19	22
TMC/MPD[h]	n_{H2O}/n_{PA}	0	2	4	5	7
0.05/0.1 wt%	ρ_{PA+H2O} (gcm^{-3})	1.26	1.35	1.42	1.42	1.54
20 min time	Swelling (%)	0	6	12	15	18
TMC/MPD[h]	n_{H2O}/n_{PA}	0	2	3	4	4
0.005/1 wt%	ρ_{PA+H2O} (gcm^{-3})	1.32	1.42	1.42	1.50	1.52
10 min time	Swelling (%)	0	2	9	9	9

When membranes are prepared at fixed reactant concentration (TMC/MPD 0.005/0.1 wt%) increasing reaction time yields a clear trend (Figure S6, Tables S1 and S2): causes polymer densification, which translates into a reduced ability to swell and uptake water (Tables S1 and S2).
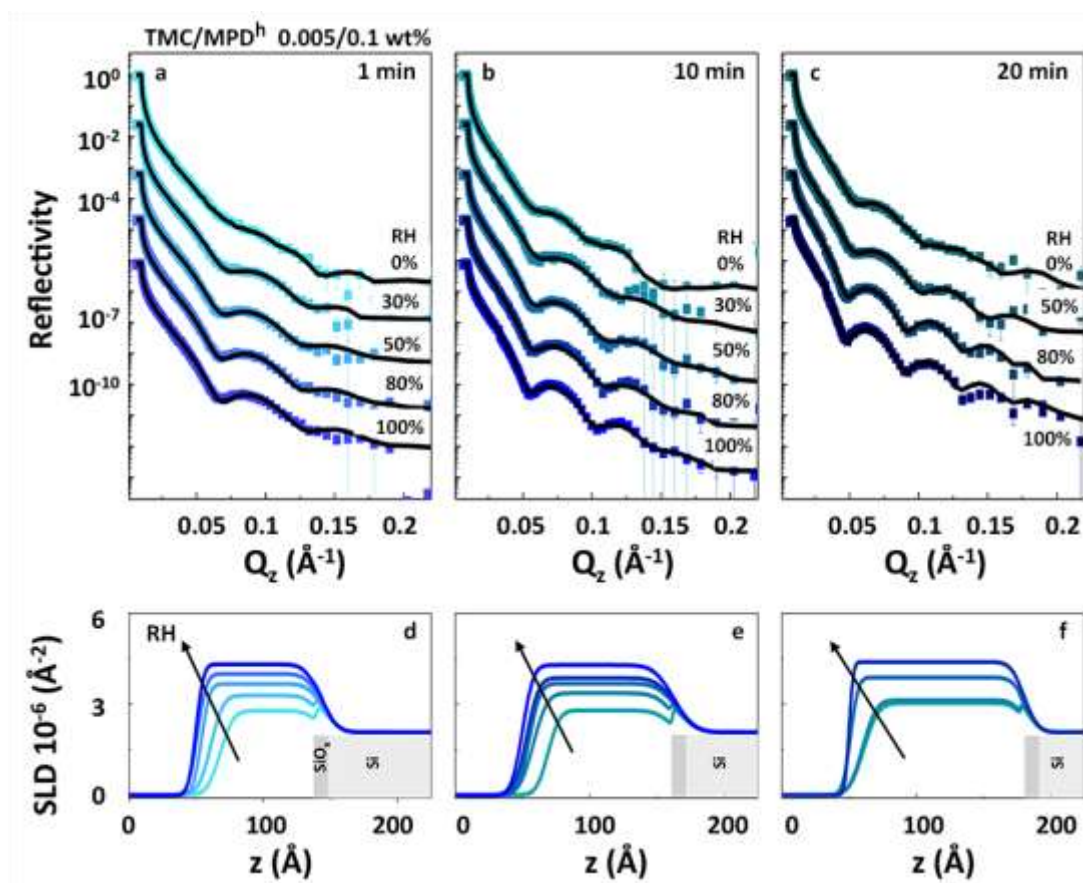
Figure S6. a-c) NR data and model fits for TMC/MPD 0.05/0.1 wt% films obtained at 10 min when hydrated at 100% RH and in direct contact to water (light and dark red, respectively). d-f) Corresponding SLD profile, where z is the distance normal to the film surface.

In agreement with NR data, XRR profiles demonstrate that the membrane hydration is a completely reversible as well as quasi-equilibrium process (Figure S7) as well as validate both thickness and surface roughness estimations benefitting from a stronger SLD contrast. Note that XRR profiles have been recorded *ex situ*, therefore the thickness of the dry membrane has been calculated by considering one-dimensional swelling (which is true in the case of a reflectivity experiment where samples have a large footprint).
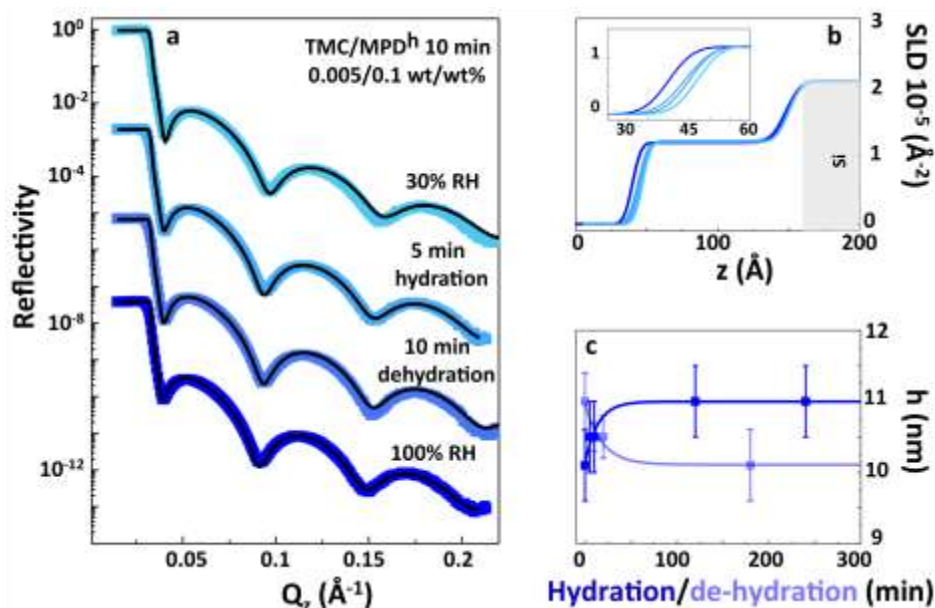
Figure S7. a) XXR data and model fits for TMC/MPD 0.005/0.1 wt% obtained at 10 min reaction times at different levels of hydration/dehydration. b) Corresponding SLD profile, where z is the distance normal to the film surface. c) Film thickness (*h*) dependence on hydration/dehydration time.

In order to confirm that our scattering profiles, recorded at 100% RH, were representative of the membrane in a fully hydrated state, additional NR experiments were performed. To reach this goal scattering profiles for the same membrane have been compared after full hydration in water vapour (100% RH) as well under immersion in water (Figure S8). The experiment confirms that the PA internal structure and water uptake are the same when the thin film is either exposed at 100% RH or in direct contact to water.
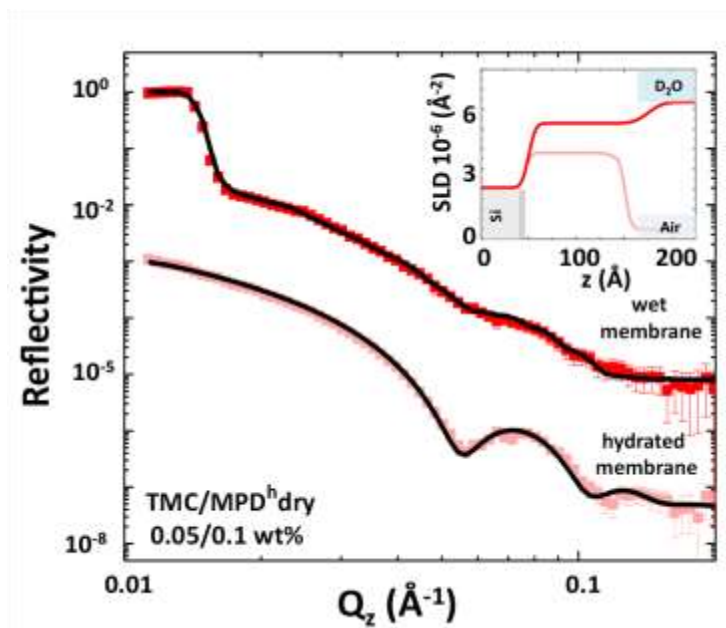
Figure S8. Comparison between NR data and model fits for TMC/MPD 0.05/0.1 wt% film when fully hydrated in water vapour (100% RH, light red curve) and dipped in water (dark red curve). In the inset are reported the corresponding SLD profiles, where z is the distance normal to the film surface.
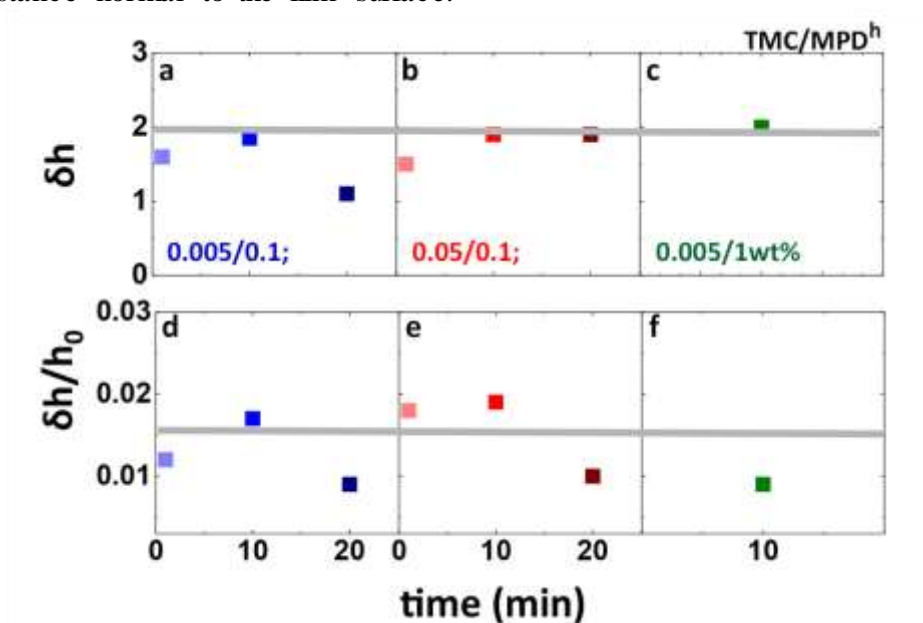

Figure S9. Comparison between the relative (δh; panels a-c) and absolute ($\delta h/h_0$; panels d-f) variation in membrane thickness as function of stoichiometry and reaction time for TMC/MPD 0.005/0.1; 0.05/0.1 and 0.005/1 wt%.
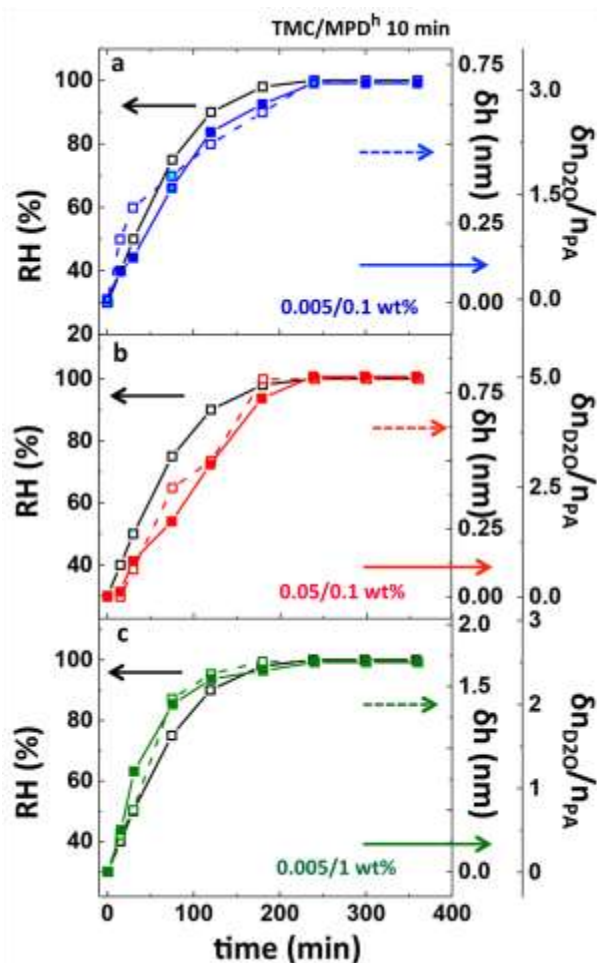
Figure S10 Comparison between the variation of water uptake (δ n_{D2O}/n_{PA}; solid line; right axis) and thickness (δh; dash line; right axis) over the time required to reach 100% of relative humidity (RH; solid line; left axis) for TMC /MPD 10 min reaction time thin films. a) Stoichiometry 0.005/0.1 wt%; b) stoichiometry 0.05/0.1 wt%; c) stoichiometry 0.005/1 wt%.

Comparison between structural parameters and performance data:

Table S3. Comparison between performance and structural data for the three stoichiometries at 10 min reaction time.

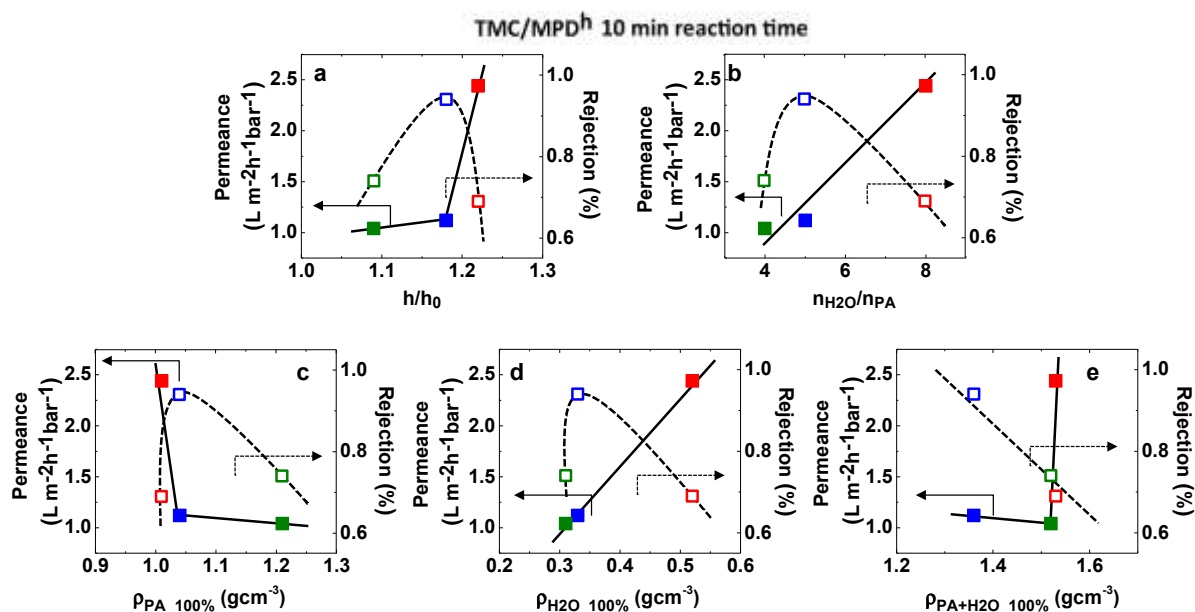| Parameter	TMC/MPD[h] 0.005/0.1 wt% 10 min time	TMC/MPD[h] 0.05/0.1 wt% 10 min time	TMC/MPD[h] 0.005/1 wt% 10 min time
Permeance (L m^{-2} h^{-1} bar^{-1})	1.12	2.44	1.04
Rejection (%)	94	69	74
Water flux (L m^{-2} h^{-1})	22.4	48.8	20.8
Permeability (L m^{-2} h^{-1} bar^{-1} m)	1.22 10^{-8}	2.66 10^{-8}	2.55 10^{-8}
h$_{100\%RH}$ (Å)	109	109	245
Swelling (%)	18	22	9
n$_{H2O}$/n$_{PA}$	5	8	4
P$_{PA+H2O}$ (gcm^{-3})	1.36	1.53	1.52

Figure S11. Variation of membrane permeance (solid points, left-hand axis) and salt rejection (open points, right-hand axis) as function of membrane structural parameters for TMC/MPD thin film prepared at 10 min reaction time (0.005/0.1; 0.05/0.1 0.005/1 wt%; blue, red and green curves, respectively). a) Variation of membrane permeance and salt rejection as function of membrane swelling. b) Variation of membrane permeance and salt rejection as function of water uptake. c) Variation of membrane permeance and salt rejection as function of polymer density at 100% RH. d) Variation of membrane permeance and salt rejection as function of water partial density at 100% RH. e) Variation of membrane permeance and salt rejection as function of total polymer density at 100% RH.

[1]   B. Khorshidi, T. Thundat, B.A. Fleck and M. Sadrzadeh, *Sci. Rep.*, 2016, **6**, 22069.

[2]   V. Freger, *Langmuir*, 2003, **19**, 4791.

[3]   S. Karan, Z. Jiang and A.G. Livingston, *Science*, 2015, **348**, 6241.

[4]   A. J. Nelson, *J. Appl. Crystallogr.* 2006, **39**, 273.

[5]   RasCal: http://sourceforge.net/projects/rscl/, accessed: May, 2015.

[6]   J. Muscatello, E.A. Müller, A.A. Mostofi and A.P. Sutton, *J. Membr. Sci*, 2017, **527**, 180.

[7]   V. Freger and S. Srebnik, *J. Appl. Polym. Sci.*, 2006, **282**, 71.

[8]   E. Harder, D.E. Walters, Y.D. Bodnar, R.S. Faibish and B. Roux, *J. Phys. Chem. B*, 2009, **113**, 10177.

[9]   R. Nadler and S. Srebnik, *J. Membr. Sci.*, 2008, **315**, 100.

[10]   S.K. Karode, S.S. Kulkarni, A.K. Suresh and R.A. Mashelkar, Chem Eng Sci, 1998, **53**, 2649.

[11]   V. Kolev and V. Freger, *Polymer*, 2014, **55,** 1420.

[12]   D.G. Cahill, V. Freger and S.Y. Kwak, *MRS Bull.*, 2008, **33**, 27.

[13]   Y. Song, P. Sun, L.L. Henry, B. Sun, *J. Membr. Sci*, 2005, **251**, 67.